Lightning Assimilation in the WRF-model (Version 4.1.1): Technique Updates and Assessment of the Applications from Regional to Hemispheric Scales

Daiwen Kang[1*], Nicholas K. Heath[2#], Robert C. Gilliam[1], Tanya L. Spero[1], and Jonathan E. Pleim[1]

[1] Center for Environmental Measurement and Modeling, Office of Research and Development, U.S. Environmental Protection Agency, Research Triangle Park, NC 27711, U.S.A.

[2] Air Quality and Atmospheric Composition, Atmospheric and Environmental Research, Lexington, MA 02421, U.S.A.

*Correspondence: kang.daiwen@epa.gov

#Currently working as an independent consultant

Abstract: The lightning assimilation (LTA) technique in the Kain-Fritsch convective

parameterization in the WRF model has been updated and applied to continental and hemispheric

simulations using lightning flash data obtained from the National Lightning Detection Network

(NLDN) and the World Wide Lightning Location Network (WWLLN), respectively. The LTA

technique uses lightning data to trigger the Kain-Fritsch convective parameterization via realistic

temperature and moisture perturbations. The impact of different values for cumulus parameters

associated with the Kain-Fritsch scheme on simulations with and without LTA were evaluated

for both the continental and the hemispheric simulations. Comparisons to gauge-based rainfall

products and near-surface meteorological observations indicated that the LTA improved the

model's performance for most variables. The simulated precipitation with LTA using WWLLN

lightning flashes in the hemispheric applications was significantly improved over the simulations

without LTA when compared to precipitation from satellite observations in the Equatorial

regions. The simulations without LTA showed significant sensitivity to the cumulus parameters

(i.e., user-toggled switches) for monthly precipitation that was as large as 40% during convective

seasons for monthly mean daily precipitations. With LTA, the differences in simulated

precipitation due to the different cumulus parameters were minimized. The horizontal grid

spacing of the modeling domain strongly influenced the LTA technique and the predicted total

precipitation, especially in the coarser scales used for the hemispheric simulation. The user-

definable cumulus parameters and domain resolution manifested the complexity of convective

process modeling both with and without LTA. These results revealed sensitivities to domain

resolution, geographic heterogeneity, and the source and quality of the lightning dataset.

1. Introduction

Thunderstorms are natural phenomena that have intrigued human imagination for thousands of years. Although early efforts in atmospheric science and modeling were focused on understanding and forecasting thunderstorms, they remain difficult to accurately simulate in meteorological models. A variety of lightning parameterization schemes have developed in regional and global atmospheric models (Price and Rind, 1992; Romps et al., 2014; Finney, 2014; Lopez, 2016) based on various physical, dynamical, and cloud properties, but these schemes marginally reproduce the spatial and temporal variability of lightning flashes with varying success over different regions of the globe. With the advancement of lightning detection technologies both at ground level and via satellite in the past decades, observed lightning flashes with coverage from regional to global scales are available and can be used for lightning assimilation (LTA). A robust LTA can improve convective simulations in meteorological models for retrospective atmospheric simulations (e.g., Heath et al., 2016; Marchand and Fuelberg, 2015) or help generate better initial fields for real-time weather forecasting (e.g., Lagouvardos et al., 2013; Giannaros et al., 2016; Fierro et al., 2012, 2015) by pinpointing where deep convection occurred and altering the meteorology in what is generally referred to as a hot start (Gan et al., 2021). In addition, lightning also profoundly impacts the chemical composition of the troposphere by generating and releasing nitrogen oxides (LNO_x) that can significantly alter ground-level ozone (O_3) concentrations in some regions (Kang et al., 2020). Because meteorological models drive air quality simulations, improving meteorological variables with LTA will cascade to chemistry fields simulated by air quality models (Allen et al., 2012; Kang et al., 2019a,b). It is especially critical when LNO_x emissions are included in air quality models, since LTA is designed to align LNO_x emissions with the time and location when atmospheric

65 convection occurred in the model, so the subsequent chemistry reactions and transport will more

66 accurately reflect the emissions from lightning (Kang et al., 2019a and 2019b).

67   Heath et al. (2016) implemented an LTA technique in the Kain-Fritsch (KF) convective

68 scheme (Kain, 2004) in the Weather Research and Forecasting (WRF) model, which extended

69 the works of Rogers et al. (2000), Mansell et al. (2007), Lagouvardos et al. (2013), and

70 Giannaros et al. (2016). In general, the lightning assimilation approach is straightforward,

71 activating deep convection where lightning is observed and only allowing shallow convection

72 where it is not. Specifically, the LTA technique uses temperature and moisture perturbations to

73 trigger KF deep convection where lightning is observed, resulting in a parameterized cloud with

74 realistic characteristics based on the local environment and our understanding of lightning-

75 producing convective clouds. It was tested using WRFv3.8 simulations for several months in

76 2011 using lightning observations from the National Lightning Detection Network (NLDN) over

77 the contiguous United States (CONUS). It was found that the simulation of warm-season rainfall

78 was substantially improved, and other near-surface meteorological variables were clearly

79 improved in retrospective WRF applications. The LTA technique has been implemented in

80 subsequent WRF releases (not publicly available yet) and applied in many meteorology and air

81 quality studies over the CONUS (e.g., U.S. EPA, 2019; Appel et al, 2021). Although using LTA

82 improved the predicted meteorological variables, some occasional unwanted departures from

83 base model predictions without LTA occurred. Most commonly, LTA resulted in a low bias in

84 summertime rainfall in some regions (U.S. EPA, 2019).

85   For this reason, it is of interest to investigate two parameters associated with the KF

86 convective scheme with different optional values, which are specified in the WRF runtime

87 namelist input file, are often encountered by WRF users

88   (https://www2.mmm.ucar.edu/wrf/users/docs/user_guide_v4/contents.html) . One parameter is

89   called kfeta_trigger (also referred to as trigger for simplicity in this paper) which controls the

90   conditions to determine how the KF convective scheme is triggered with three optional values: 1,

91   the default value; 2, moisture-advection based trigger (only for ARW - the advanced research

92   WRF dynamical solver); and 3, RH-dependent additional perturbation to Option 1 (not tested).

93   Another parameter is called cudt (namely **cu**mulus time interval, **d**elta **t**) and its value determines

94   the minutes between cumulus physics calls (here it is the KF scheme). The default value of 0

95   indicates that the cumulus physics is called at every model step, and any non-zero value specifies

96   the interval (minutes) that the cumulus physics is called (for example, cudt=10 means that the

97   cumulus physics is called every 10 minutes). Even though there are some discussions and

98   recommendations regarding the choice of these parameter values through online forums or WRF

99   user mailing list (e.g., https://forum.mmm.ucar.edu/; https://wrfems.info/;

100   https://www.epa.gov/sites/default/files/2017-02/documents/wrf_with_ltga_userguide.pdf), but

101   there is no literature evaluating how these parameter values impact model performance when

102   LTA is used.

103   The applications and evaluations of the LTA technique were limited to the CONUS,

104   reflecting the areal coverage of NLDN (Murphy et al., 2021). As the spatial applications of

105   atmospheric composition modeling are expanded from regional to hemispheric and global scales

106   and new lightning datasets are available, there is a strong need to examine how this LTA

107   technique performs at these larger scales when lightning flash data from a less accurate detection

108   network are used. Thus, lightning flashes from the World Wide Lightning Location Network

109   (WWLLN, operated by the University of Washington: http://www.wwlln.com) is a suitable

110 candidate because it has the global coverage, albeit its detection efficiency is lower than the

111 >95% of NLDN for cloud-to-ground (CG) flashes (Abarca et al., 2010).

112   Our research has multiple objectives based on the aforementioned open research needs:

113 1) assess the impact of the parameter values associated with the KF convective scheme on WRF

114 performance over the CONUS domain without LTA (BASE case) and with LTA using lightning

115 flashes from NLDN; 2) examine the LTA in WRF using lightning flashes from WWLLN and

116 compare to the simulations with NLDN lightning flashes; and 3) apply LTA to WRF simulations

117 over the Northern Hemisphere and evaluate the performance in terms of precipitation and near-

118 surface meteorological variables. In section 2, we describe the updates made to the initial LTA

119 technique (Heath et al., 2016). Section 3 provides the detailed data and methodologies of the

120 model simulations and their evaluation. Section 4 presents our analysis on the impact of

121 parameters with KF convective schemes with and without lightning assimilation over CONUS

122 using lightning flashes from NLDN and WWLLN. In section 5, we analyze the use of lightning

123 flashes from WWLLN for LTA and evaluate WRF simulations with and without LTA over the

124 Northern Hemisphere. And we conclude with key findings and recommendations in section 6.

125 **2. Updates on the LTA technique**

126   The lightning assimilation used here is based on Heath et al. (2016), and a full description

127 of the method can be found in Heath et al. Here, we provide only the essential details, along

128 with recent modifications to the scheme.

129   First, the lightning data (WWLLN or NLDN) is binned to the WRF domain in both time

130 and space. The temporal binning is done every 30 min and includes lightning data from -10 min

131 to +20 min of the current time. The spatial regridding searches for a lightning strike within each

132 grid box (using the staggered grid edge coordinates) within each time bin. This process creates a

133 new lightning file with the same horizontal dimensions as the WRF domain filled with zeros (no

134 lightning) or ones (lightning) at each 30-minute time step. During the WRF simulation, if

135 lightning is present, the scheme first goes through its standard updraft calculations, except that it

136 uses the layer with the greatest moist static energy as its updraft source layer (USL). If the

137 resulting cloud does not meet the criteria for deep convection, 0.1 g kg^{-1} of water vapor and 0.1

138 K are incrementally added to the USL until deep convection is forced. In the original Heath et

139 al. scheme, only moisture was added to the USL. We have included temperature perturbations to

140 further promote activating deep convection in these grid points with lightning.

141   In the unmodified KF scheme, a cloud must exceed a minimum depth (as a function of

142 cloud base temperature) to satisfy the deep convection criteria. Specifically, a cloud base

143 temperature greater than 20ºC must have a cloud greater than 4 km deep. For a cloud base

144 temperature less than 0ºC, the cloud depth only needs to be 2 km. For cloud bases between 0 –

145 20ºC, the minimum cloud depth is defined as $2000 + 100 T_{LCL}$, where T_{LCL} is the temperature at

146 the lifted condensation level (LCL) (Kain 2004). Heath et al. (2016) modified this depth for

147 lightning assimilation to be more consistent with lightning-producing storms. Specifically,

148 within WRF, storms with a base temperature greater than or equal to 20ºC must have a cloud

149 depth of at least 6 km with a cloud top temperature less than -20ºC. Similarly, in the original

150 model in Heath et al., storms with a cloud base temperature less than 20ºC must have a cloud

151 depth of at least 4 km and a cloud top temperature less than -20ºC. These criteria were set to

152 ensure that sub-grid deep convective clouds were deep enough to have a mixed-phase layer to

153 support lightning (e.g., Mansell et al., 2007; Bruning et al., 2014; Preston and Fuelberg, 2015).

154 In this study, we slightly modified the scheme to require that the cloud top is at least one model

155   level above the -20ºC level, ensuring cloud-top temperatures are less than -20ºC (e.g.,

156   Stolzenburg and Marshall, 2009). The prior limit at -20ºC could inadvertently weaken simulated

157   deep convective clouds, which may contribute to the dry bias in earlier applications of lightning

158   assimilation approaches (U.S. EPA, 2019).

159   In Heath et al. (2016), if deep convection could not be achieved after incrementally

160   adding up to 1 g kg^{-1} to the USL (which is now 1 g kg^{-1} and 1 K in our update), then no further

161   action was taken, and deep convection was not activated by KF. However, to increase the

162   realism of the scheme and increase the odds of deep convection the next time the scheme is

163   called, we have updated the approach as follows. If a deep convective cloud cannot be activated,

164   the tallest cloud created is passed into the KF shallow convection scheme. In the KF scheme,

165   shallow clouds are re-diagnosed each time the scheme is called. For example, suppose a shallow

166   cloud is generated at t=0 and KF is called at 5 min intervals. In that case, at the t=5 min call, KF

167   would determine if a shallow cloud is still present. Thus, the cloud can evolve so that at t=5 min

168   it could have slightly different characteristics than the one diagnosed at t=0. This allows shallow

169   clouds to grow, decay, or persist at short timescales.

170   Therefore, if the LTA method cannot trigger deep convection, the shallow cloud that is

171   generated within WRF can precondition the atmosphere, thus increasing the likelihood of deep

172   convection the next time the KF scheme with LTA is called. Therefore, these refinements to the

173   LTA scheme in KF more closely replicate how convective initiation is observed in nature, where

174   shallow cumulus and congestus clouds precondition the environment prior to deep convection

175   initiation.

176   Lastly, at grid points without observed lightning, deep convection is suppressed in WRF,

177   and only the shallow portion of KF is allowed to run (this is referred to as the "ShallowOnly"

178   method). Because convective clouds in nature can form and precipitate without generating

179   lightning, this suppression technique serves as a realistic approach to reproduce nature given the

180   constraints of the KF parameterization.

181

182   **3. Data and Methodology**

183   3.1. Lightning flash data

184   Lightning flash data from two ground-based lightning detection networks were used for the

185   assimilation using the LTA technique in this study. The NLDN provides cloud-to-ground

186   lightning observations with a detection efficiency of >95% and a location accuracy of about 150

187   m (Murphy et al., 2021) over the contiguous U.S. (CONUS). The WWLLN provides global

188   lightning data with lower detection efficiency and location accuracy (Abarca et al., 2010;

189   Rudlosky and Shea, 2013; Burgesser, 2017) compared to NLDN and the Lightning Imaging

190   Sensor (LIS) observations (Mach et al., 2007). Since WWLLN has global coverage, even with its

191   relatively lower detection efficiency and location accuracy compared to NLDN, it could be a

192   good option for applications beyond CONUS. Figure 1 shows how the average lightning flash

193   rate (flashes $km^{-2}hr^{-1}$) from WWLLN compares to NLDN during July and September 2016 when

194   hourly lightning flash counts are gridded into the CONUS 12-km grid cells.

195   As shown in Figure 1, the lightning flash rates in NLDN are much higher than those in

196   WWLLN, especially during July and over the land, and this is generally true (not shown) that

197   NLDN reported more lightning flashes than WWLLN during warm months over land. The

198   differences are much smaller during cool months and over the coastal regions where NLDN has

199   coverage. Note that the absolute difference in flash count may not necessarily translate

200   proportionally into convective activities in terms of LTA because the LTA technique as

201 described in Heath et al. (2016) depends on the detection of lightning occurrence (binary "yes"

202 or "no" situation), not the actual flash count, in a specific time interval at a grid cell.

203 3.2. Precipitation Data

204   The daily precipitation from the Parameter-elevation Regressions on Independent Slopes

205 Model (PRISM)'s high-resolution spatial climate data for the United States

206 (https://climatedataguide.ucar.edu/climate-data/prism-high-resolution-spatial-climate-data-

207 united-states-maxmin-temp-dewpoint) is used to evaluate WRF-simulated precipitation over the

208 CONUS, and the NOAA Climate Prediction Center (CPC)'s global unified gauge-based analysis

209 of daily precipitation (https://psl.noaa.gov/data/gridded/data.cpc.globalprecip.html) product is

210 employed to assess WRF's hemispheric precipitation predictions. The daily total PRISM

211 precipitation data are available at 4-km horizontal grid spacing over the CONUS, and the annual

212 CPC precipitation (partitioned into daily totals) is available globally at 0.5° latitude × 0.5°

213 longitude grid (720 × 360) resolution. These datasets were regridded to the WRF modeling

214 domains for the 12-km CONUS and the 108-km Northern Hemisphere to pair with model

215 simulations in time and space. To assess the simulated precipitation over the oceans, especially

216 in the tropical regions where no gauge-based measurement is available, products from the Global

217 Precipitation Measurement (GPM) (Huffman et al., 2015; Asong et al., 2017), a joint mission co-

218 led by NASA and the Japan Aerospace Exploration Agency (JAXA) and comprised of an

219 international network of satellites that provide the next-generation global observations of rain

220 and snow, are employed. The Integrated Multi-satellitE Retrievals for GPM (IMERG) Long-term

221 Precipitation Data Products

222 (https://arthurhouhttps.pps.eosdis.nasa.gov/gpmdata/YYYY/MM/DD/imerg/; registration is

223 required for access) cover the entire globe with 0.1° latitude × 0.1° longitude grid resolution. To

224   compare with WRF simulated hemispheric precipitation, the daily mean precipitation data from

225   the IMERG V06 dataset (https://gpm.nasa.gov/data/directory) from 2016 is regridded onto the

226   hemispheric WRF domain. The research-quality gridded IMERG V06 dataset Final Run product

227   estimates precipitation using quasi-Lagrangian time interpolation, gauge data, and climatological

228   adjustment.

229   3.3. Ground-Based Meteorological Data

230   The impacts of user-definable parameter values associated with KF and datasets for LTA

231   were quantified for simulated near-surface meteorological variables such as precipitation, 2-m

232   temperature (T2), water vapor mixing ratio, wind speed and wind direction. The simulated

233   meteorological fields from WRF are compared against observations from NOAA National

234   Centers for Environmental Information (NCEI) land-based stations, which are archived from

235   data collected globally (https://www.ncei.noaa.gov/products/land-based-station). The

236   Atmospheric Model Evaluation Tool (AMET) (Appel et al., 2011) is used to pair surface

237   observations with model predicted values in both space (bilinear interpolation) and time (hourly).

238   3.4. Model Configurations and Simulation Details

239   The WRF model (Skamarock and Klemp, 2008) version 4.1.1 (WRFv411,

240   https://github.com/wrf-model/WRF/releases/tag/v4.1) with LTA updates to Heath et al. (2016)

241   (as described in Section 2) is used to perform simulations over the CONUS and the hemispheric

242   domains. The CONUS domain is configured with 36 vertical levels and 12-km horizontal grid

243   spacing with 472×312 grid points. The hemispheric domain is configured with 45 vertical

244   levels and 108-km horizontal grid spacing with 200×200 grid points that covers the entire

245   Northern Hemisphere and the northern border of the Southern Hemisphere along the Equator.

246   The simulation period for CONUS simulations is from April–July in 2016 with 10-day spin-up

247 period from March 22; for the hemispheric domain, annual simulations for 2016 are performed.

248 Our analysis focuses on July when convective activities are often the most prevalent over the

249 CONUS; other months are examined in the hemispheric simulations which simulate the year-

250 round convective activities in the tropics. The detailed configurations of cloud microphysics,

251 land surface parameters, radiation schemes, and four-dimensional data assimilation (FDDA) are

252 the same as described in Heath et al. (2016) and sample WRF namelist input files for both the

253 CONUS and hemispheric simulations are included in the supplementary information (Table S1

254 and Table S2). Data assimilation in the form of FDDA more specifically follows Heath et al.

255 (2016) with updates noted in Gilliam et al. (2021) for the hemispheric domain where ~28 km

256 NCEP Global Forecast System (GFS) analyses were used to nudge tropospheric temperature,

257 moisture, and wind above the planetary boundary layer. For the CONUS domain the same

258 nudging was applied, but 12 km North American Mesoscale (NAM) model analyses were

259 leveraged. These two analysis datasets are a blend of short-term forecast with a comprehensive

260 set of surface, upper-air, radar, aircraft, satellite, and other observations like sea-surface

261 temperature that represent the best guess of the state of the atmosphere at any given time.

262   The KF scheme includes two options to trigger convective activity. Trigger 1 is based on

263 a mass-conservative cloud model, which includes parameterized moist downdrafts, entrainment,

264 and detrainment at the cloud edge (Kain and Fritsch, 1990, 1993) and allows interaction between

265 cloud and environment, and it is the default option for most applications. Trigger 2 is an alternate

266 option based on Ma and Tan (2009), and that is a moisture-advection modulated trigger function

267 to improve results in subtropical regions when large-scale forcing is weak. In addition, the KF

268 scheme is called by default at every time step, but it can be configured to only update convective

269 parameters on a user-definable time increment. In this study, sensitivities are conducted to the

270   version of the KF trigger (i.e., Trig1 and Trig2, abbreviated as K1 and K2 in Table 1,

271   respectively), as well as to frequency at which KF is called (i.e., "cudt"). Two sensitivities on

272   cudt were performed: one where KF is called at each model integration time step (i.e., "Cudt0",

273   abbreviated as C0 in Table 1), and the other where KF is updated every 10 minutes of integration

274   time (i.e., "Cudt10", abbreviated as C10 in Table 1). The time step is 1 minute (Table S1) and 3

275   minutes (Table S2) for the CONUS and hemispheric WRF simulations, respectively. The

276   sensitivities to KF trigger and update frequency are combined in a matrix of simulations that also

277   are conducted with/without LTA, and they are listed in Table 1. All eight simulations are

278   performed for both the CONUS and the hemispheric domains. For LTA cases, lightning flashes

279   from both NLDN and WWLLN are used over the CONUS domain and lightning flashes from

280   WWLLN are used for the hemispheric domain. For convenience of description, the cases without

281   LTA are collectively referred to as BASE cases, and the cases with LTA are referred to as LTA

282   cases. To further distinguish the lightning networks, the LTA cases are also referred to as LTA

283   NLDN (or simply NLDN) and LTA WWLLN (or simply WWLLN) cases, respectively.

284   3.5. Evaluation Methodologies

285   The assessment of the impact of LTA on model performance is focused on precipitation

286   since that is the most affected variable, though other near-surface variables are also evaluated.

287   Due to the highly heterogeneous nature of thunderstorms and lightning over space, in addition to

288   examining the overall statistics across the modeling domain, statistics are analyzed to assess the

289   impact of LTA over U.S. climate regions (https://www.ncei.noaa.gov/monitoring-

290   references/maps/us-climate-regions) in both domains and some of the larger countries in the

291   hemispheric simulations. Figure 2 shows these climate regions over the CONUS modeling

292 domain and the selected countries (also referred to as regions) in the hemispheric modeling

293 domain.

294   The statistical metrics in this analysis include the widely used correlation coefficient (r)

295 to measure the linear association of measured and simulated variables, mean bias (MB) and

296 normalized mean bias (NMB) to quantify the departure of simulated values from measured

297 values, and root mean square error (RMSE) and normalized mean error (NME) to elucidate the

298 errors associated with model simulations. More emphasis is placed on certain metrics than others

299 depending on the nature of the simulated quantity. For instance, with precipitation, correlation

300 coefficient (if the model can simulate rainfall at the right time and location) and MB and NMB

301 (if the model over- or under-estimate rainfall amount) are more straightforward than the error

302 metrics (though they are still relevant), but MB and NMB are inappropriate to evaluate wind

303 directions.

304

305 **4. CONUS WRF Simulations**

306   As shown in Table 1, four BASE (without LTA) cases, four LTA cases using lightning flash

307 data from NLDN, and four LTA cases using lightning flash data from WWLLN over the

308 CONUS domain were performed using the combinations of two trigger options and two

309 convective update (cudt) intervals, respectively. For the LTA cases, when lightning flashes were

310 not present, the ShallowOnly option (Heath et al., 2016) was used (Table S1).

311 4.1. Precipitation

312   Figure 3 displays the July 2016 mean statistics generated by pairing the gridded WRF

313 precipitation with the values from PRISM in time and space for each of the U.S. climatological

314 regions. As shown in Figure 3, the BASE simulations present the more dramatic fluctuations

315   among cumulus parameter sensitivities than the LTA cases. With Trig1, when the cudt is

316   changed from 0 to 10, the correlation coefficient is substantially reduced across all the regions

317   (Figure 3a), and increases in biases (overestimate of precipitation, Figures 3b&c) and errors

318   (Figures 3d&e) are also worsened by less frequent cumulus updates. With trigger 2, the biases

319   (MB and NMB) changed from overestimation to underestimation, and the errors (RMSE and

320   NME) were smaller compared to Trig1. Though the setting for cudt altered simulations with

321   Trig2, the difference was smaller than the cases with Trig1. In general, the Trig1 cases tended to

322   produce more precipitation (overestimate compared to PRISM precipitation) than the Trig2 cases

323   (underestimate compared to PRISM precipitation), and the Cudt10 cases generated more

324   precipitation than the Cudt0 cases. Among the four cases in the BASE model simulations, the

325   K1C0 case (Trig1, Cudt0) is the most favorable in terms of the correlation coefficients and

326   precipitation biases, but the error statistics, especially NME, may not be the most desirable.

327   Using LTA (Figure 3), the correlation coefficients significantly increased over the

328   domain and across the regions (from the range of ~0.25 to ~0.40 to the range of ~0.30 to ~0.48)

329   relative to the BASE cases. Though the LTA WWLLN cases had lower correlation compared to

330   the LTA NLDN cases due to the lower detection efficiency of lightning flashes in WWLLN, the

331   improvement was still rather considerable compared to the BASE cases. The biases in the LTA

332   NLDN cases are most favorable with values negative but closest to zero (small underestimate).

333   The LTA WWLLN cases produced larger negative biases than the BASE cases and LTA NLDN

334   cases, again, related to detection efficiency of the networks. All the LTA cases (both NLDN and

335   WWLLN) produced smaller errors than the BASE cases, and the differences between the NLDN

336   cases and WWLLN cases were minimal. Comparing the LTA cases with the BASE cases, one

337   noticeable feature is that with the different trigger and cudt values, all the statistics fluctuated

338   dramatically from one case to another in the BASE cases, but fluctuation among the LTA cases

339   was minimized and negligible. This is expected, as the moisture and temperature perturbations

340   used to trigger convection with LTA (Section 2) will take precedence over the trigger options

341   and grouping the lightning data into 30-minute bins should mitigate the influence of the cudt

342   option. These features were deliberately incorporated into the LTA technique for precisely these

343   reasons, but this paper documents their systematic testing.

344   Examination of the statistics across the climatological regions over the CONUS domain

345   indicates that the Ohio Valley (OVC) stands out among all the regions with the lowest

346   correlation coefficients and largest RMSE values in all the BASE cases. However, with LTA, the

347   correlation coefficients in OVC were brought to the median range among other regions, though

348   the RMSE values were still the largest in that region; these features in OVC are more

349   understandable as manifested in Figure 12, examined in detail in Section 5. Other statistics in

350   OVC with LTA were comparable with other regions except for relatively larger negative MB

351   values associated with the LTA WWLLN cases. Another obvious characteristic with regards to

352   correlation coefficients and errors (RMSE and NME) was that there was more spread among the

353   regions in the LTA cases than in the BASE cases (except in OVC), which resulted from the

354   geographically heterogeneous nature of convective precipitation and the associated observed

355   lightning intensity across the regions.

356   To alleviate the underestimation of precipitation in the LTA WWLLN cases, additional

357   simulations (K1C10Ws0 and K2C10Ws0; where K1C10W and K2C10W are the same as in

358   Table 1, while s0 means zero suppress when lightning flash is not present) were performed by

359   switching the suppression option as described in Heath et al. (2016) from "ShallowOnly" to

360   "NoSuppress." This modification still triggers deep convection where lightning is observed;

361   however, at grid points without lightning, the KF scheme is configured to run normally (i.e., the

362   same as in the BASE cases). As shown in Figure S1, the correlation coefficients in the

363   WWLLN+s0 cases were comparable with other LTA cases, and the values in the K2C10Ws0

364   case were similar to the NLDN cases and improved upon the K1C10W case. The MB in the

365   WWLLN+s0 cases were mostly positive (overestimate), which is expected because the KF

366   scheme has more freedom to activate deep convection. The K2C10Ws0 case produced the most

367   desirable results (domain mean MB is nearly zero) among all the cases. However, the biases

368   associated with LTA simulations using the "NoSuppress" option are affected by both the

369   lightning detection efficiency and the domain resolutions, which is more evident in the LTA

370   simulations over the hemispheric domain in Section 5.

371   4.2. Other Near-Surface Meteorological Variables

372   Besides precipitation, T2, water vapor mixing ratio, wind speed, and wind direction are

373   also analyzed. As shown in Figure 4, T2 in the BASE cases has correlation coefficients over the

374   CONUS domain and all the regions ranging from ~0.95–0.98. With LTA, the correlations for T2

375   were further improved for all the regions, with WWLLN cases performing slightly worse than

376   the NLDN cases. The impact of cumulus parameters on correlations was minimal for the BASE

377   and LTA cases. However, the cumulus parameters seem to impact the biases (MB and NMB,

378   Figures 4b,c) and errors (RMSE and NME, Figure 4d,e) in the BASE cases across all the regions,

379   and like precipitation, all the LTA cases minimized the impact of different cumulus parameter

380   values. All the LTA cases reduced the errors (RMSE and NME) associated with T2 across all the

381   regions, with NLDN slightly better than WWLLN. In summary, the T2 statistics were improved

382   by using LTA, and the WWLLN cases were comparable to the NLDN cases with a slight

383   degradation for all the regions.

384   The 2-m water vapor mixing ratios metrics (Figure 5) of the cases, in general, resemble

385   those of T2, in that the LTA cases have slightly increased the correlation coefficients from the

386   already well-simulated BASE cases. More spread occurs for biases (MB and NMB, Figures 5b,c)

387   and within the BASE cases for errors (RMSE and NME, Figures 5d,e). Regional spread in these

388   statistics is attributed to the diverse air mass types that drive large differences in the moisture

389   content and convective activity. Even though the values were low for both errors and biases (<

390   0.5%), using either LTA technique is an improvement over the BASE cases.

391   The cumulus parameters and LTA showed less impact on the correlations for 10-m wind

392   speed, but the impacts on biases and errors were noticeable (Figure 6). All the model cases

393   underestimate wind speed (~5–12%, depending on regions and model cases), and the cumulus

394   parameters caused relatively large differences in the metrics of the BASE cases with both trigger

395   and cudt options contributing most. Overall, using Trig2 with Cudt10 is most favorable in terms

396   of biases (less underestimate) and errors (smaller errors) among the BASE cases. In all the LTA

397   cases, the underestimation was reduced when compared to the BASE cases, and errors were

398   reduced with negligible differences among the cases with different cumulus parameters and

399   assimilating lightning data from the different networks. Similar behavior was observed for wind

400   direction where only correlation coefficient, MB, and RMSE are displayed in Figure S2 because

401   normalized metrics do not apply.

402

403   **5. Northern Hemispheric WRF Simulations**

404   As shown in Table 1, the model cases performed over the Northern Hemisphere are

405   similar to those performed over the CONUS, but with LTA cases using lightning data from

406   WWLLN that was gridded on the domain with 108-km horizontal grid spacing.

5.1. Precipitation

Before comparing the simulated precipitation with available observations, the examination begins with how the WRF-simulated precipitation with and without LTA compares spatially over the Northern Hemisphere. Figure 7 displays the mean daily precipitation during July 2016 from two LTA cases and two BASE cases (Trig1 and Trig2) and the corresponding differences between LTA and BASE (LTA – BASE) cases with the same trigger values, and Figure S3 presents the mean daily precipitation differences between HK1C0W and HK1C0B cases throughout 2016. Compared to the BASE cases, the LTA cases produced significantly less rainfall along the Equatorial regions but generally more rainfall away from the Equator, especially over the midlatitude land regions. Because no gauge-based observational data are available over the ocean, the IMERG precipitation for July 2016 is presented in Figure 7g with the difference plots from the base case (HK1C0B) and the LTA case (HK1C0W) being displayed in Figures 7h and 7i, respectively. Over the Equatorial regions, the precipitation simulated by the LTA cases (Figures 7b and 7e) more closely resembled the IMERG precipitation than the BASE cases. The difference plots clearly indicate that the base cases significantly overestimated, and the LTA cases slightly underestimated the precipitation over large areas in the Equatorial regions. Similar results persisted throughout the year as shown in Figure S4 (the difference of mean daily precipitation by month between the base case, HK1C0B, and the IMERG product) and Figure S5 (the difference of mean daily precipitation by month between the LTA case, HK1COW, and the IMERG product). Next, the WRF simulated precipitation is compared with the CPC gauge-based analysis values over land. Figure 8 displays the CPC rainfall and simulated mean daily precipitation during July 2016 along with the estimates from the LTA and BASE cases with different cumulus parameters. Since the gauge-based observational values are only available over land, the simulated values in Figure 8

430 are only displayed over land. As shown in Figure 8, all the model cases simulated the overall

431 spatial pattern of higher values in the tropical regions and lower values in high latitude regions.

432 However, subtle differences existed from case to case in different regions. For example, the

433 HK1C10B case (Figure 8d) and the HK2C10B case (Figure 8f) produced the highest and the lowest

434 precipitation over Africa and South America (along the Mexico coast to the South American

435 continent) within the modeling domain.

436 All the LTA cases uniformly produced larger correlation coefficients than the BASE

437 cases (Figure 9) when and where convective activities were prevalent. In the U.S., convective

438 activities occur during warm months (from May to September), while in Mexico and India,

439 convection is active throughout the year. In Canada, convective activities are less frequent

440 because of the cooler temperatures and low moisture at the high latitude. When and where

441 convection was active, the cumulus parameters produced significant differences in modeled

442 convective activity, as correlation coefficients are higher in the BASE cases with Trig1. Same as

443 the simulations over the CONUS domain, the cumulus parameters had a minor impact on the

444 correlation coefficients for the LTA cases regardless the regions. This indicates that, even with

445 the less dense WWLLN lightning observations, using LTA improves the timing and location of

446 deep convection.

447 RMSE were comparable for all the model cases across the selected regions (Figure 10),

448 with the LTA cases pointing to lower values than the BASE cases at all the regions except for the

449 U.S. where the LTA and BASE cases alternated to have slightly lower RMSE values over each

450 other during the year. Alternatively, the MB values varied significantly among the model cases

451 and across the regions as shown in Figure 11. One common feature is that the differences among

452 the LTA cases were small, but two distinctly separate groups among the BASE cases were noted

453 in all the regions; the cases with Trig1 had always significantly greater precipitation values than

454 the cases with Trig2. In China and Mexico, all the simulations overestimated the precipitation

455 through the year except for small underestimate during the cool months (October–December). In

456 India, the overestimate and underestimate were equally split among the model cases, with

457 dramatic changes from month to month in the same model case. The behavior of MB values

458 among the model cases and through the year was more stable for the U.S. (to a lesser extent in

459 Canada) than in other regions, in which the BASE cases with Trig1 have the best performance

460 (MB values near zero), the BASE cases with Trig2 significantly underestimated precipitation

461 over land during convective season, and all the LTA cases overestimated precipitation over land

462 during the warm months. Here we offer two plausible explanations for the drastically different

463 behaviors of the MB values associated with precipitation in different regions.

464   First, from the modeling point of view, the WRF model is widely studied and applied in

465 North America, especially in the U.S. As a result, more accurate observation-based datasets are

466 available to nudge WRF through FDDA (Liu et al., 2008), and all the work has led to the best

467 performance over the U.S. for the recommended default set of convective trigger and update

468 frequency for the cumulus scheme. Second, from the observational point of view, the CPC

469 rainfall dataset is built upon field gauge measurements that may vary in accuracy and

470 consistency from county to county. As shown in Figure S6, the NMB values were generally in

471 the range of -50% to 50% in the U.S. and Canada (comparable to the NMB values for the 12-km

472 CONUS simulations against PRISM precipitation as shown in Figure 3c), but in other countries,

473 especially during cool months, the values were up to hundreds or even thousands of percent that

474 suggests possible few observations available in the denominator in NMB calculations. For

475   instance, the highest NMB value in China coincided with the Spring Festival that is often a long

476   holiday for China suggesting possible gaps for data collection.

477   We next focus on the high MB values associated with the LTA cases in the U.S.

478   Consistent in the analysis in Figure 3b, the LTA WWLLN cases over the 12-km CONUS domain

479   always had larger negative MB (underestimates) than the LTA NLDN cases due to the lower

480   detection efficiency of lightning flashes in WWLLN than in NLDN. However, in the 108-km

481   hemispheric simulations, the same WWLLN datasets produced large positive MB

482   (overestimates) for precipitation. To understand this phenomenon, we need to first examine how

483   the LTA method works. Because it uses a yes/no lightning indicator to trigger convection, 108-

484   km grid spacing might be too coarse for such a simplistic approach to work. For example, one

485   lightning strike within a 108-km grid cell will trigger deep convection, which, because of the

486   large spatial coverage of the grid cell, can contribute to the high bias in precipitation because

487   convective rainfall is realistically more localized. Although the KF scheme sets a fixed radius

488   for thunderstorms (e.g., Equation 6 in Kain 2004), applying the resulting rain over the entire 108-

489   km × 108-km grid box could partially explain the excess rainfall. This may also be explained by

490   the fact that the convective time-scale formulation in KF scheme was originally developed at

491   grid lengths of 20–25 km (Sims et al., 2017). A potential developmental pathway for the LTA

492   method at these scales is to test different thresholds of the 30-min flash density to ensure

493   sufficient lightning is present to trigger deep convection. Overall, compared to the CPC rainfall,

494   the LTA technique significantly improved the temporal and spatial correlation of convective

495   precipitation, but the precipitation amount was overestimated over the U.S. and other regions for

496   the 108-km modeling domain.

497   To further examine the impact of modeling domain resolutions on convective

498   precipitation, Figure 12 displays the spatial precipitation from PRISM, CPC (regridded onto the

499   12-km CONUS domain), and simulated precipitation from one BASE case and two LTA cases

500   with NLDN and WWLLN data, respectively, over the 12-km CONUS domain and one LTA case

501   over the 108-km hemispheric domain that has been regridded to the 12-km CONUS domain. As

502   shown in Figures 12a,b, the two observation-based precipitation products, PRISM and CPC,

503   compared well to each other, noting that the PRISM product displays more subtle granularity

504   than the CPC product due to the large difference in spatial resolutions (4-km for PRISM versus

505   0.5° for CPC). The overall spatial pattern of mean daily precipitation was captured by both the

506   12-km LTA simulations (Figures 12d,e), and the 108-km LTA simulation (Figure 12f). The

507   heaviest rainfall was centered in the OVC area in the observation-based and the simulated

508   precipitation maps, but the shape and spread of the rain band were different. The rain band in the

509   12-km BASE case (Figure 12c) was more spread and scattered with southwest-to-northeast

510   orientation, while the observation-based products and the LTA cases indicated a relatively

511   smaller area with west-east direction. Thus, the LTA cases (12-km CONUS simulations)

512   compared better to the observation-based products spatially than the BASE case. The K2C10W

513   case (with WWLLN) tended to produce less precipitation than the K2C10N case (with NLDN)

514   and both observation-based products. These spatial discrepancies for precipitation in OVC

515   between PRISM and the model cases were reflected by the unique statistical behavior as

516   displayed in Figure 3 and discussed in Section 4.1. As a likely artifact of excessively activated

517   convection within the 108-km grid cells with a spatial scale much larger than most thunderstorm

518   scales, the HK2C10W case indicated areas of heavy precipitation that were also shown in the

519   observation-based products and the 12-km LTA cases (both K2C10W and K2C10N) at

520 approximately same locations but with much less spatial extent. To resonate with the large

521 discrepancies in the MB values shown in Figure 11a among the BASE cases, the precipitation

522 from HK2C10B and HK2C10B cases is similarly displayed in Figures 12g,h. The case with

523 Trig1 was clearly more comparable to the CONUS cases than the Trig2 case in that the

524 precipitation from Trig2 was severely underestimated across the entire U.S. These hemispheric

525 simulations amplified the impact of the trigger options on precipitation during warm months

526 among the BASE cases, resulting in differences in daily total precipitation of up to 40% in the

527 U.S. (Figure S6a). These results underscore the need to carefully set cumulus parameters for the

528 KF scheme in WRF simulations.

529   The mismatch of the spatial scales between domain resolution and thunderstorms in the

530 108-km simulations is a limitation of current LTA scheme that could be improved in future

531 development. In addition to using lightning density to trigger convection, another option is to

532 implement the LTA scheme in the MultiScale Kain-Fritsch (MSKF) scheme (Glotfelty et al.,

533 2019; Zheng et al., 2016), a "scale-aware" variant of KF that refines the convective tendencies

534 based on the grid spacing used in the simulation.

535 5.2. Impact on Other Meteorological Variables

536   The impact of the cumulus parameters and LTA scheme on near-surface meteorological

537 variables of the 108-km hemispheric simulations are evaluated like the 12-km CONUS

538 simulations. However, due to the lack of observation data beyond North America, the analysis is

539 mainly focused on the U.S. regions, but all the available data within the hemispheric domain is

540 collectively referred to as "ALL" regardless of where the data originated. Affected by the coarser

541 domain resolution, all the statistical measures for T2 (Figure 13) from the hemispheric

542 simulations indicated degradations in model performance relative to the 12-km CONUS domain

543   (Figure 4). As in the CONUS simulations, the LTA cases increased correlation coefficients and

544   decreased errors (RMSE and NME) compared to the BASE cases. Like the CONUS simulations,

545   the cumulus parameters minimally affected the LTA cases, while significant deviations were

546   produced among the BASE cases. Unlike the CONUS simulations where both trigger and cudt

547   contributed to T2 differences, the large differences among the BASE cases for the hemispheric

548   simulations were attributed to the trigger options. Though all the cases tended to underestimate

549   T2 (contrary to the CONUS simulations where T2 was generally overestimated), among the

550   BASE cases, greater underestimates were associated with Trig1 than Trig2. The LTA cases

551   uniformly underestimated T2 consistent with the Trig1 BASE cases. The performance of

552   hemispheric simulations for 2-m water vapor mixing ratio (Figure 14) resembles T2 in the

553   comparison to the CONUS simulations (Figure 5), which produced smaller correlation

554   coefficients and larger errors and biases (mainly overestimates for both CONUS and hemispheric

555   simulations). Without exception, the LTA cases consistently performed better in terms of

556   correlation coefficients and errors than the BASE cases. However, different from other

557   meteorological variables, the MB and NMB associated with water vapor mixing ratio are

558   affected by both cumulus parameters (trigger and cudt) for all the model cases (both BASE cases

559   and LTA cases). The LTA cases with Trig1 performed better than the cases with Trig2, and with

560   the same trigger value, cudt=0 is preferable to cudt=10; however, for the BASE cases, it was the

561   opposite, though with smaller differences. At the 108-km grid spacing, the 10-m wind speed

562   (Figure S7) and wind direction (not shown) statistics were comparable among the cumulus

563   parameters and the application of LTA.

564

565   **6.   Discussion and Recommendations**

566   This study corroborated that the simple observation-based LTA scheme implemented in

567   Heath et al. (2016) improved WRF simulated precipitation and other near-surface meteorological

568   variables as evidenced by the simulations over multiple spatial scales and over a longer test

569   period. Testing on a 12-km CONUS domain using lightning flashes from WWLLN instead of

570   NLDN slightly reduced the correlation coefficients and locally increased errors due to the lower

571   detection efficiency of WWLLN. The update of the LTA technique reduced the underestimate of

572   precipitation that was often reported in the application of WRF simulations conducted over the

573   CONUS domain (U.S. EPA, 2019). Changing lightning flash data from NDLN to WWLLN

574   resulted in additional underestimate of precipitation due to fewer lightning flashes in WWLLN

575   than the NLDN dataset. However, when the WWLLN data was used in the hemispheric

576   simulations, the model performance for precipitation over the Equatorial regions was

577   significantly improved from significant overestimation in the base cases to slight

578   underestimation in the LTA cases, and the precipitation over land was generally overestimated

579   during the convective season for almost all the selected regions, especially over North America.

580   The application of LTA in the hemispheric simulations with a 108-km domain exposed a

581   shortcoming of this simple LTA scheme. When the model grid cell is substantially larger than

582   most thunderstorm scales (Murphy and Konrad II, 2005), over-triggering of convection within the

583   entire grid cell leads to overestimated precipitation. With the current LTA implementation and

584   the high lightning detection efficiency network, such as NLDN, the 12-km grid spacing is

585   suitable for LTA because thunderstorms often have a radial distance of 1–10 km. When lightning

586   data from low detection efficiency networks (such as WWLLN) are used over finer resolution

587   domains (≤12 km), the "NoSuppress" option with LTA could balance increasing precipitation

588   while maintaining reasonable levels of uncertainty in the other variables for a more holistic

589   model evaluation. The effect of domain resolution on precipitation simulation with LTA

590   portends further development and improvement of the LTA technique. Two potential

591   developmental directions are to use criteria values of lightning flash density dependent on grid

592   resolution to trigger deep convection and/or to implement the LTA scheme in the MSKF scheme

593   in WRF to adapt to different simulation scales. Preliminary experimentation on the 108-km scale

594   (not shown) suggests that MSKF could improve these comparisons with observations (compared

595   to the KF scheme presented here), including better cloud and precipitation fields (Hogrefe et al.,

596   2021).

597   The experiment of cumulus parameters (trigger and cudt) associated with the KF scheme was

598   performed for both the CONUS and hemispheric WRF simulations. Results revealed several key

599   behaviors in both the BASE case simulations and LTA case simulations. First, the BASE case

600   simulations were sensitive to both trigger and cudt options over the CONUS domain, but only

601   trigger options produced significant variations for the hemispheric simulations. Second, the

602   impact of the cumulus parameters on LTA cases was insignificant for both modeling domains.

603   Separately, the original LTA technique as described in Heath et al. (2016) showed influence

604   from the cumulus parameters on the LTA cases (Figure S8), but after implementing the updated

605   cloud top height (one model level above -20° C) and the additional pre-conditioning shallow

606   convection (see Section 2), the fluctuations among the LTA cases were significantly reduced.

607   Third, the most pronounced impact of cumulus parameters was on the amount of precipitation in

608   the BASE cases. The Trig1 option generated up to a 10% overestimate of month-mean daily

609   precipitation over the CONUS with cudt=0 and an additional 10–15% overestimate with cudt=10

610   during July 2016. With Trig2, the simulated precipitation became underestimated by about 10–

611   15%, with the cudt contributing to ~5% difference; Cudt10 had less underestimate than Cudt0.

612 However, over the hemispheric domain, only the trigger option dramatically affected simulated

613 precipitation; during the summer months (June, July, and August), the Trig2 cases

614 underestimated the mean daily precipitation by up to 40% more than the Trig1 cases that

615 matched the observation-based precipitation products within 10%. In summary, without LTA,

616 the recommended default values (trigger=1 and cudt=0) by WRF documentation remain the best

617 option for both the CONUS and hemispheric simulations to achieve the best model performance,

618 especially for North America, and with LTA, all the options performed equally well.

619 As one of the most prominent meteorological models, WRF has been widely used in a variety

620 of applications from regional to global scales and from weather and climate studies to air

621 pollution transport in air quality forecast and regulatory compliances. It is important to improve

622 the convective processes (e.g., convective transport of air pollutants matching the times and

623 locations of lightning NO_x production) to have more accurate precipitation and other

624 meteorological fields with more resources being available including observational datasets,

625 computing capability, and advanced scheme development. Observation-based data assimilation

626 has been historically proven to be one of the most effective methods to improve model's

627 performance in time and space. This research is emerging to consider and use the lightning

628 observations that have become available in various formats and scales in the past decades to

629 improve convection simulations through LTA. Additional networks of lightning observations

630 and more detailed properties associated with the process of lightning discharge are becoming

631 available (such as the strokes per flash, the strength of lightning energy level, and the separation

632 of cloud-to-ground and inter- or intra-cloud strikes being more accurately quantified, especially

633 with the available satellite lightning products from Geostationary Lightning Mapper (GLM)

634 detection systems borne on the GOES-16 and -17 satellites (Goodman et al., 2013)).

635   Accordingly, lightning assimilation techniques will continue to evolve and build upon the

636   research presented here.

637

Code and data availability

The WRF model is available for download through the WRF website (http://www.wrf-model.org/index.php). The LTA code is not publicly available yet but interested users can contact the corresponding author to acquire the source code. The raw lightning flash observation data can be purchased through Vaisala Inc. (https:// www.vaisala.com/en/products/systems/lightning-detection), and the WWLLN raw data are also available for purchase at http://wwlln.net. The immediate data except the lightning flash data behind the figures are available from doi: https://doi.org/10.5281/zenodo.6493145. PRISM Precipitation data for the United States are retrieved from https://climatedataguide.ucar.edu/climate-data/prism-high-resolution-spatial-climate-data-united-states-maxmin-temp-dewpoint and the CPC Global Unified Precipitation data provided by the NOAA/OAR/ESRL PSL, Boulder, Colorado, USA, from their Web site at https://psl.noaa.gov/data/gridded/data.cpc.globalprecip.html. The IMERG data were provided by the NASA/Goddard Space Flight Center's Precipitation Measurement Missions (PMM) Science Team and Precipitation Processing System (PPS), which develop and compute the IMERG as a contribution to GPM, and archived at the NASA GES DISC.

Author contributions. DK conceptualized the study, performed the model simulation and data curation, carried out the analysis, and wrote the paper. NH developed the mechanism and software and wrote the paper. RG prepared the scripts for model simulations and data analysis and edited the paper. TS supervised the research, provided resources, and edited the paper. JP edited the paper.

Competing interests. The authors declare that they have no conflict of interest.

Disclaimer: This paper has been subjected to an EPA review and approved for publication. The views expressed here are those of the authors and do not necessarily reflect the views or policies of the U.S. Environmental Protection Agency (EPA).

Acknowledgement:

We thank Jerry Herwehe and Kiran Alapaty at the EPA for reviewing the paper and providing valuable comments and suggestions. We give our sincere thanks to Dr. Lisa Neef and the other anonymous referee for their comments and many suggested changes that improved the clarity and readability of this paper.

References

Abarca, S. F., Corbosiero, K. L., and Galarneau Jr., T. J.: An evaluation of the Worldwide Lightning

   Location Network (WWLLN) using the National Lightning Detection Network (NLDN) as ground

   truth, J. Geophys. Res., 115, D18206, doi:10.1029/2009JD013411, 2010.

Allen, D. J., Pickering, K. E., Pinder, R. W., Henderson, B. H., Appel, K. W., and Prados, A.: Impact of

   lightning-NO on eastern United States photochemistry during the summer of 2006 as determined

   using the CMAQ model, Atmos. Chem. Phys., 12, 1737–1758, 2012.

Appel, K. W., Gilliam, R. C., Davis, N., Zubrow, A., and S. C. Howard, S. C.: Overview of the

   Atmospheric Model Evaluation Tool (AMET) v1.1 for evaluating meteorological and air quality

   models, Environ. Modell. Software, 26, 434–443, doi:10.1016/j.envsoft.2010.09.007, 2011.

Appel, K. W., Bash, J. O., Fahey, K. M., Foley, K. M., Gilliam, R. C., Hogrefe, C., Hutzell, W. T., Kang,

   D., Mathur, R., Murphy, B. N., Napelenok, S. L., Nolte, C. G., Pleim, J. E., Pouliot, G. A., Pye, H.

   O., Ran, L., Roselle, S. J., Sarwar, G., Schwede, D. B., Sidi, F. L., Spero, T. L., and Wong, D. C.: The

   Community Multiscale Air Quality (CMAQ) model versions 5.3 and 5.3.1: system updates and

   evaluation, Geosci. Model Dev., 14, 2867–2897, https://doi.org/10.5194/gmd-14-2867-2021, 2021.

Asong, Z. E., Razavi, S., Wheater, H. S., and Wong, J. S.: Evaluation of Integrated Multisatellite

   Retrievals for GPM (IMERG)over Southern Canada against Ground Precipitation Observations:A

   Preliminary Assessment, J. Hydrometeorology, 18, 1033-1050, https://doi.org/10.1175/JHM-D-16-

   0187.1, 2017.

Bruning, E. C., Weiss, S. A., and Calhoun, K. M.: Continuous variability in thunderstorm primary

   electrification and an evaluation of inverted-polarity terminology, Atmos. Res., 135–136, 274–284,

   doi:10.1016/j.atmosres.2012.10.009, 2014.

Burgesser, R. E.: Assessment of the World Wide Lightning Location Network (WWLLN) detection

   efficiency by comparison to the Lightning Imaging Sensor (LIS), Q. J. R. Meteorol. Soc. 143: 2809–

   2817, doi:10.1002/qj.3129, 2017.

696   Fierro, A. O., Mansell, E. R., Ziegler, C. L., and MacGorman, D. R.: Application of a lightning data

697   assimilation technique in the WRFARW model at cloud-resolving scales for the tornado outbreak of

698   24 May 2011, Mon. Weather Rev., 140, 2609–2627, 2012.

699   Fierro, A. O., Clark, A., Mansell, E. R., MacGorman, D. R., Dembek, S. R., and Ziegler, C. L.: Impact of

700   storm-scale lightning data assimilation on WRF-ARW precipitation forecasts during the 2013 warm

701   season over the contiguous United States, Mon. Weather Rev., 143, 757–777, 2015.

702   Finney, D. L., Doherty, R. M., Wild, O., Huntrieser, H., Pumphrey, H. C., and Blyth, A. M.: Using cloud

703   ice flux to parametrise large-scale lightning, Atmospheric Chemistry and Physics, 14 (23),

704   12,66512,682, doi:10.5194/acp-14-12665-2014, 2014.

705   Gan, R., Yang, Y., Xie, Q., Lin, E., Wang, Y., and Liu, P.: Assimilation of Radar and Cloud-to-Ground

706   Lightning Data Using WRF-3DVar Combined with the Physical Initialization Method—A Case

707   Study of a Mesoscale Convective System. J. Meteorol. Res. 35, 329–342.

708   https://doi.org/10.1007/s13351-021-0092-4, 2021.

709   Giannaros, T. M., Kotroni, V., and Lagouvardos, K.: WRF-LTNGDA: A lightning data assimilation

710   technique implemented in the WRF model for improving precipitation forecasts, Environ. Modell.

711   Software, 76, 54–68, 2016.

712   Gilliam, R. C., Herwehe, J. A., Bullock, Jr, O. R., Pleim, J. E., Ran, L., Campbell, P. C., & Foroutan, H.:

713   Establishing the suitability of the model for prediction across scales for global retrospective air

714   quality modeling. J. Geophys. Res.: Atmospheres, 126, e2020JD033588,

715   https://doi.org/10.1029/2020JD033588, 2021.

716   Glotfelty, T., Alapaty, K., He, J., Hawbecker, P., Song, X., and Zhang, G.: The Weather Research and

717   Forecasting Model with Aerosol–Cloud Interactions (WRF-ACI): Development, evaluation, and

718   initial application, Mon. Wea. Rev., 147, 1491–1511, doi:10.1175/MWR-D-18-0267.1, 2019.

719   Goodman, S. J., Blakeslee, R. J., Koshak, W. J., Mach, D., Baiely, J., Buechler, D., Carey, L., Schultz, C.,

720   Bateman, M., McCaul Jr., E., and Stano G.: The GOES-R Geostationary Lightning Mapper (GLM),

721   Atmos. Res., 125-126, 34-49, doi: 10.1016/j.atmosres.2013.01.006, 2013.

722   Heath, N. K., Pleim, J. E., Gilliam, R. C., and Kang, D.: A simple lightning assimilation technique for

723   improving retrospective WRF simulations, J. Adv. Model. Earth Syst., 8, 1806–1824,

724   https://doi.org/10.1002/2016MS000735, 2016.

725   Hogrefe, C., Gilliam, R., Mathur, R., Henderson, B., Sarwar, G., Appel, K. W., Pouliot, G., Willison, J.,

726   Miller, R., Vukovich, J., Eyth, A., Talgo, K., Allen, C., and Foley, K.: CMAQv5.3.2 ozone

727   simulations over the Northern Hemisphere: model performance and sensitivity to model

728   configuration. 20th Annual CMAS Conference, November 1–5, 2021, Virtual, 2021.

729   Huffman, G. J., Adler, R. F., and Nelkin, E. J.: Integrated Multi-satellitE Retrievalsfor GPM (IMERG)

730   technical documentation. NASA/GSFC Code612 Tech. Doc., 48 pp. [Available online at

731   http://pmm.nasa.gov/sites/default/files/document_files/IMERG_doc.pdf.], 2015.

732   Kain, J. S.: The Kain-Fritsch convective parameterization: An update, J. Appl. Meteorol., 43(1), 170–181,

733   doi:10.1175/1520-0450(2004)043<0170:TKCPAU>2.0.CO;2, 2004.

734   Kain, J.S. and Fritsch, J. M.: A one-dimensional entraining/detraining plume model and its application in

735   convective parameterization, J. Atmos. Sci., 47, pp. 2784-280,1990.

736   Kain, J.S. and Fritsch, J. M.: Convective parameterization for mesoscale models: the Kain–Fritsch

737   scheme, The Representation of Cumulus Convection in Numerical Models, Meteor. Monogr., No. 46,

738   Amer. Meteor. Soc., pp. 165-170, 1993.

739   Kang, D., Mathur, R., Pouliot, G. A., Gilliam, R. C., and Wong, D. C.: Significant ground-level ozone

740   attributed to lightning-induced nitrogen oxides during summertime over the Mountain West States,

741   npj Climate and Atmospheric Science 3, doi: 10.1038/s41612-020-0108-2, 2020.

742   Kang, D., Pickering, K., Allen, D., Foley, K., Wong, D., Mathur, R., and Roselle, S.: Simulating

743   Lightning NO Production in CMAQv5.2: Evolution of Scientific Updates, Geosci. Model Dev. 12,

744   3071-3083, https://doi.org/10.5194/gmd-12-3071-2019, 2019a.

745   Kang, D., Foley, K., Mathur, R., Roselle, S., Pickering, K., and Allen, D.: Simulating Lightning NO

746   Production in CMAQv5.2: Performance Evaluations, Geosci. Model Dev. 12, 4409–4424,

747   https://doi.org/10.5194/gmd-12-4409-2019, 2019b.

748   Lagouvardos, K., Kotroni, V., Defer, E., and Bousquet, O.: Study of a heavy precipitation event over

749   southern France, in the frame of HYMEX project: Observational analysis and model results using

750   assimilation of lightning, Atmos. Res., 134, 45–55,2013.

751   Liu, Y., Warner, T. T., Bowers, J. F., Carson, L. P., Chen, F., Clough, C. A., Davis, C.A., Egeland, C. H.,

752   Halvorson, S. F., Huck Jr., T. W., Lachapelle, L., Malone, R. E., Rife, D. L., Sheu, R. -S., Swerdlin,

753   S. P., and Weingarten, D. S.: The operational mesogamma-scale analysis and forecast system of the

754   U. S. Army Test and Evaluation Command. Part 1: Overview of the modeling system, the forecast

755   products, J. Appl. Meteorol. Climatol., 47, 1077–1092, 2008.

756   Lopez, P.: A lightning parameterization for the ECMWF Integrated Forecasting System, Monthly

757   Weather Review, 144 (9), 30573075, doi:10.1175/mwr-d-16-0026.1, 2016.

758   Ma, L.-M., and Tan, Z. M.: Improving the Behavior of the Cumulus Parameterization for Tropical

759   Cyclone Prediction: Convection Trigger. Atmospheric Research, 92, 190-211.

760   https://doi.org/10.1016/j.atmosres.2008.09.022, 2009.

761   Mach, D. M., Christian, H. J., Blakeslee, R. J., Boccipio, D. J., Goodman, S. J., and Boeck, W. L.:

762   Performance assessment of the Optical Transient Detector and Lightning Imaging Sensor, J. Geophys.

763   Res.,112, D09210, doi:10.1029/2006JD007787, 2007.

764   Mansell, E. R., Ziegler, C. L., and MacGorman, D. R.: A lightning data assimilation technique for

765   mesoscale forecast models, Mon. Weather Rev., 135, 1732–1748, doi:10.1175/MWR3387.1, 2007.

766   Marchand, M. R., and Fuelberg, H. E.: Assimilation of lightning data using a nudging method involving

767   low-level warming, Mon. Weather Rev., 142, 4850–4871, doi:10.1175/MWR-D-14-00076.1., 2015.

768   Murphy, M. J., Cramer, J. A., and Said, R. K.: Recent history of upgrades to the U.S. National Detection

769   Network, J. Atmos. Ocean. Tech., 38, 573-581, doi:10.1175/JTECH-D-19-0215.1, 2021.

770   Murphy, M. S., and Konrad II, C. E.: Spatial and temporal patterns of thunderstorm events that produce

771   cloud-to-ground lightning in the interior southeastern United States, Monthly Weather Review, 133,

772   1417-1420,2005.

773   Preston, A. D., and Fuelberg, H. E.: Improving lightning cessation guidance using polarimetric radar data,

774   Weather Forecasting, 30, 308–328, doi:10.1175/WAF-D-14-00031.1, 2013.

775   Price, C., and Rind D.: A simple lightning parameterization for calculating global lightning distributions,

776   Journal of Geophysical Research: Atmospheres, 97 (D9), 99199933, doi:10.1029/92jd00719, 1992.

777   Rogers, R. F., Fritsch, J. M., and Lambert, W. C.: A simple technique for using radar data in the dynamic

778   initialization of a mesoscale model, Mon. Weather Rev., 128, 2560–2574, 2000.

779   Romps, D. M., Seeley, J. T., Vollaro, D., and Molinari, J.: Projected increase in lightning strikes in the

780   United States due to global warming, Science, 346 (6211), 851854, doi:10.1126/science.1259100,

781   2014.

782   Rudlosky, S. D., and Shea, D. T.: Evaluation WWLLN performance relative to TRMM/LIS, Geophys.

783   Res. Lett., 40, 2344-2348, doi:10.1002/grl.50428, 2013.

784   Sims, A. P., Alapaty, K., and Raman, S.: Sensitivities of Summertime Mesoscale Circulations in the

785   Coastal Carolinas to Modifications of the Kain-Fritsch Cumulus Parameterization, Mon. Wea. Rev.,

786   145, 4381-4399, doi:10.1175/MWR-D-16-0047.1, 2017.

787   Skamarock, W. C., and Klemp, J. B.: A time-split nonhydrostatic atmospheric model, Journal of

788   Computational Physics, 227, 3465-3485, doi:10.1016/j.jcp.2007.01.037, 2008.

789   Stolzenburg, M., and Marshall, T. C.: Electric field and charge structure in lightning-producing clouds,

790   Lightning: Principles, Instruments and Applications, H.-D. Betz, U. Schumann, P. Laroche (Eds.),

791   641 pp., Springer, doi:10.1007/978-1-4020-9079-0_3, 2009.

792   U.S. EPA: Meteorological Model Performance for Annual 2016 Simulation WRF v3.8, EPA-454/R-19-

793   010, https://www.epa.gov/sites/default/files/2020-10/documents/met_model_performance-

794   2016_wrf.pdf, 2019.

795   Zheng, Y., Alapaty, K., Herwehe, J. A., Del Genio, A. D., and Niyogi, D.: Improving high-

796   resolution weather forecasts using the Weather Research and Forecasting (WRF) Model with

797   an updated Kain–Fritsch scheme, Mon. Wea. Rev., 144, 833–860, doi:10.1175/MWR-D-15-

798   0005.1, 2016.

799

800

Table 1. Model Cases used in this study. The case names are comprised of elements from the other four columns, which describe the simulation domain (blank = CONUS, H = hemispheric), the version of the Kain-Fritsch trigger that was applied (trigger 1 = K1, trigger 2 = K2), the frequency that the convective properties was updated (every time step = C0, every 10 minutes = C10), and the lightning data that were assimilated in the simulation (B = Base/none, N = NLDN, W = WWLLN).

Case Name	Domain (none or H)	trigger (K1 or K2)	cudt (C0 or C10)	LTA Network (B, N, W)
K1C0B	CONUS	1	0	Base/none
K1C10B	CONUS	1	10	Base/none
K2C0B	CONUS	2	0	Base/none
K2C10B	CONUS	2	10	Base/none
K1C0N	CONUS	1	0	NLDN
K1C10N	CONUS	1	10	NLDN
K2C0N	CONUS	2	0	NLDN
K2C10N	CONUS	2	10	NLDN
K1C0W	CONUS	1	0	WWLLN
K1C10W	CONUS	1	10	WWLLN
K2C0W	CONUS	2	0	WWLLN
K2C10W	CONUS	2	10	WWLLN
HK1C0B	Hemisphere	1	0	Base/none
HK1C10B	Hemisphere	1	10	Base/none
HK2C0B	Hemisphere	2	0	Base/none
HK2C10B	Hemisphere	2	10	Base/none
HK1C0W	Hemisphere	1	0	WWLLN
HK1C10W	Hemisphere	1	10	WWLLN
HK2C0W	Hemisphere	2	0	WWLLN
HK2C10W	Hemisphere	2	10	WWLLN

807

808

809
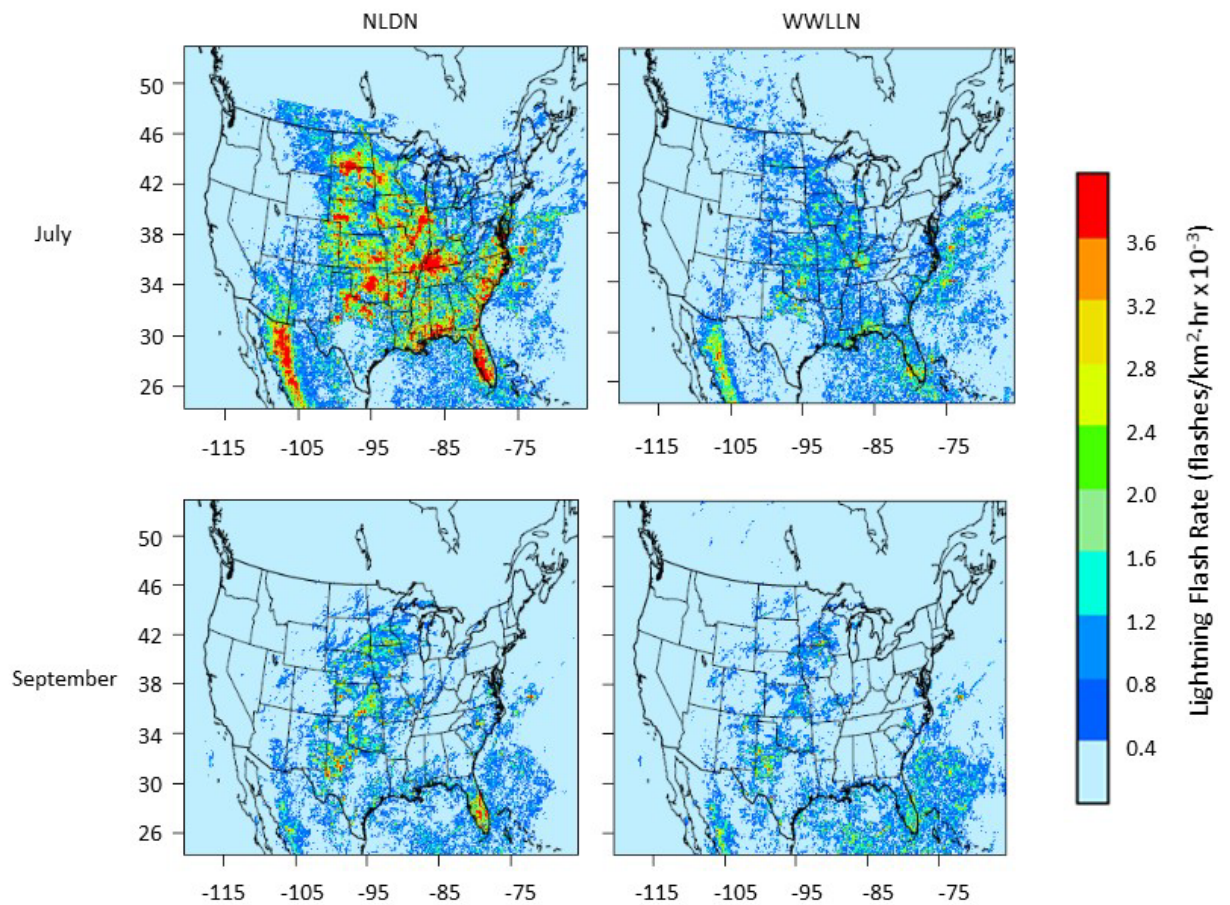
810

811   **Figure 1.** The mean hourly lightning flash rate from NLDN and WWLLN over the 12km

812   CONUS domain in July and September 2016.

813
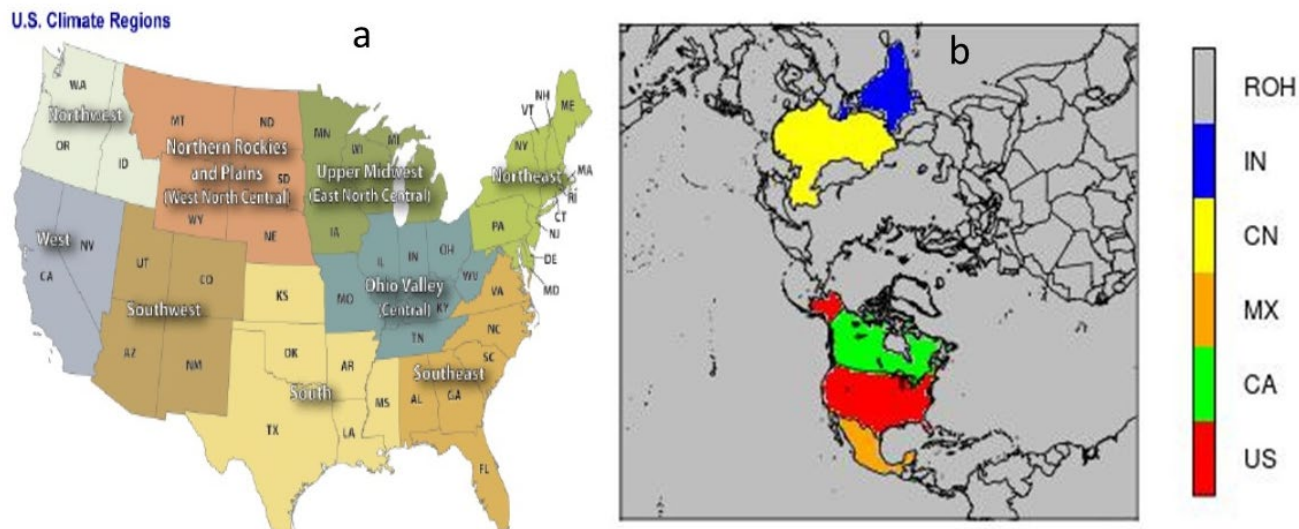
814   **Figure 2.** Analysis Regions (Countries), a. the climate regions in the CONUS, and b. the

815   countries over the northern hemisphere – US: United States; CA: Canada; MX: Mexico; CN:

816   China; IN: India; ROH: Other countries/regions except the five specific countries in the

817   hemispheric domain. The U.S. climate regions are: Northeast (NE), Southeast (SE), Ohio Valey

818   Central (OVC), Upper Midwest (UM), South, West North Central (WNC), Southwest (SW),

819   Northwest (NW), and West.

820

821

822
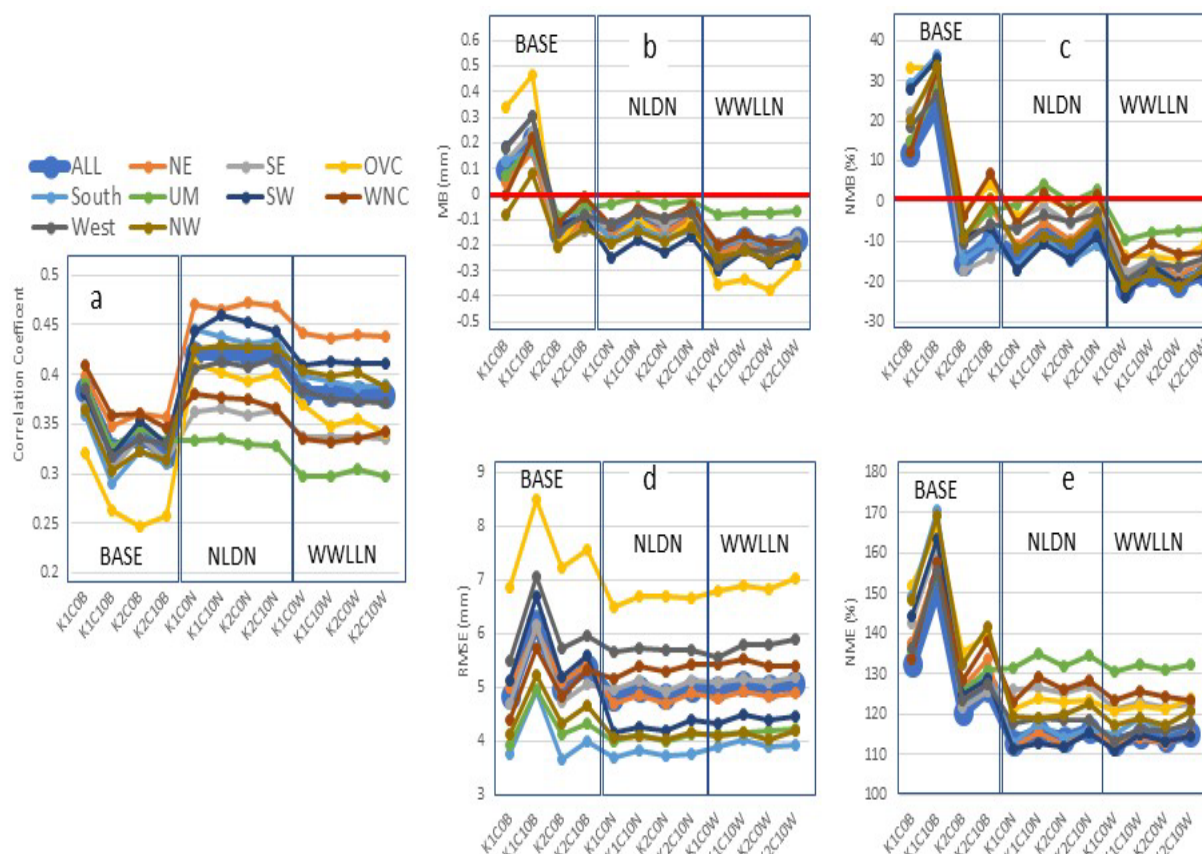
Figure 3. Monthly mean statistics for precipitation from BASE and LTA simulations

comparing to the values from PRISM for the modeling domain and the climatological

regions over the CONUS, respectively, during July 2016: a) correlation coefficient, b) MB,

c) NMB, d) RMSE, and e) NME. In each plot, there are three sets of simulations (BASE,

LTA with NLDN, and LTA with WWLLN) and each having four cases from the

combinations of cumulus parameters.

829

830

831
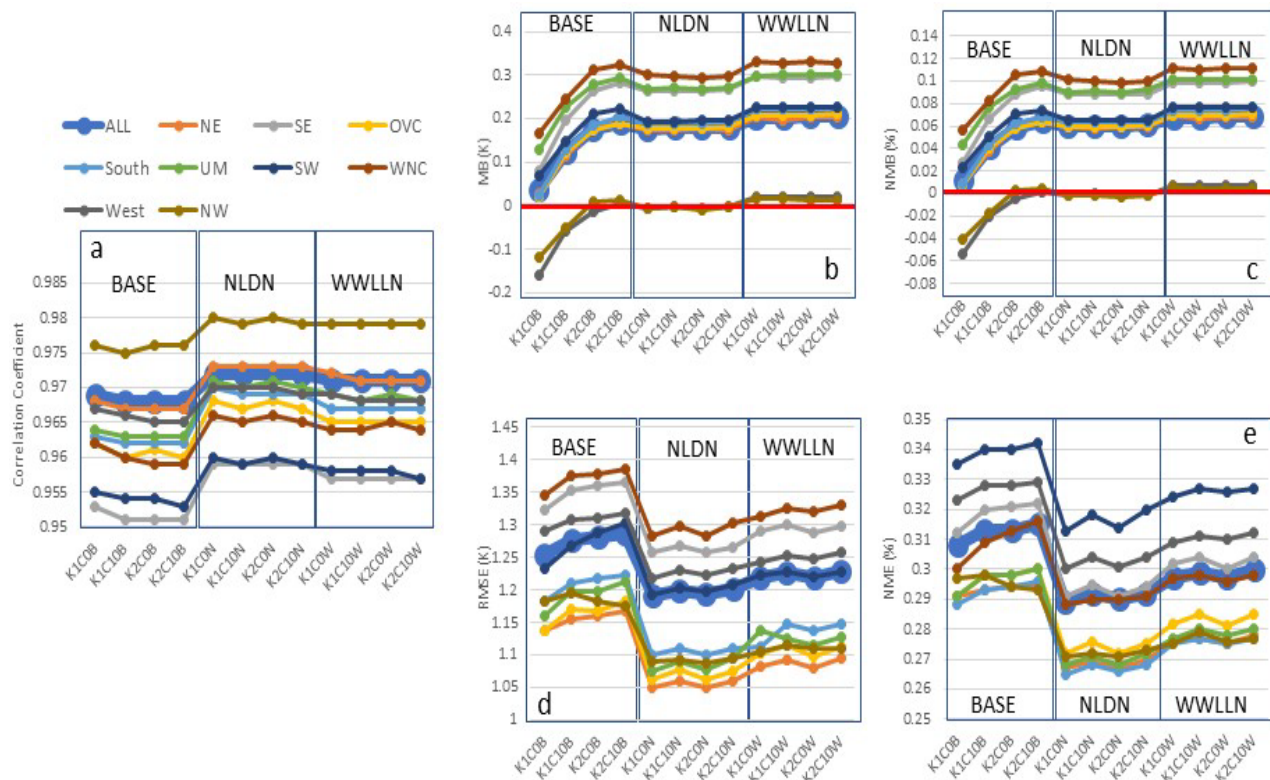
Figure 4. Same as Figure 3, but for 2-m temperature (T2) in that the simulated T2 values are paired with observations from NCEI's land-based stations in time and space (hourly mean values).

835

836

837
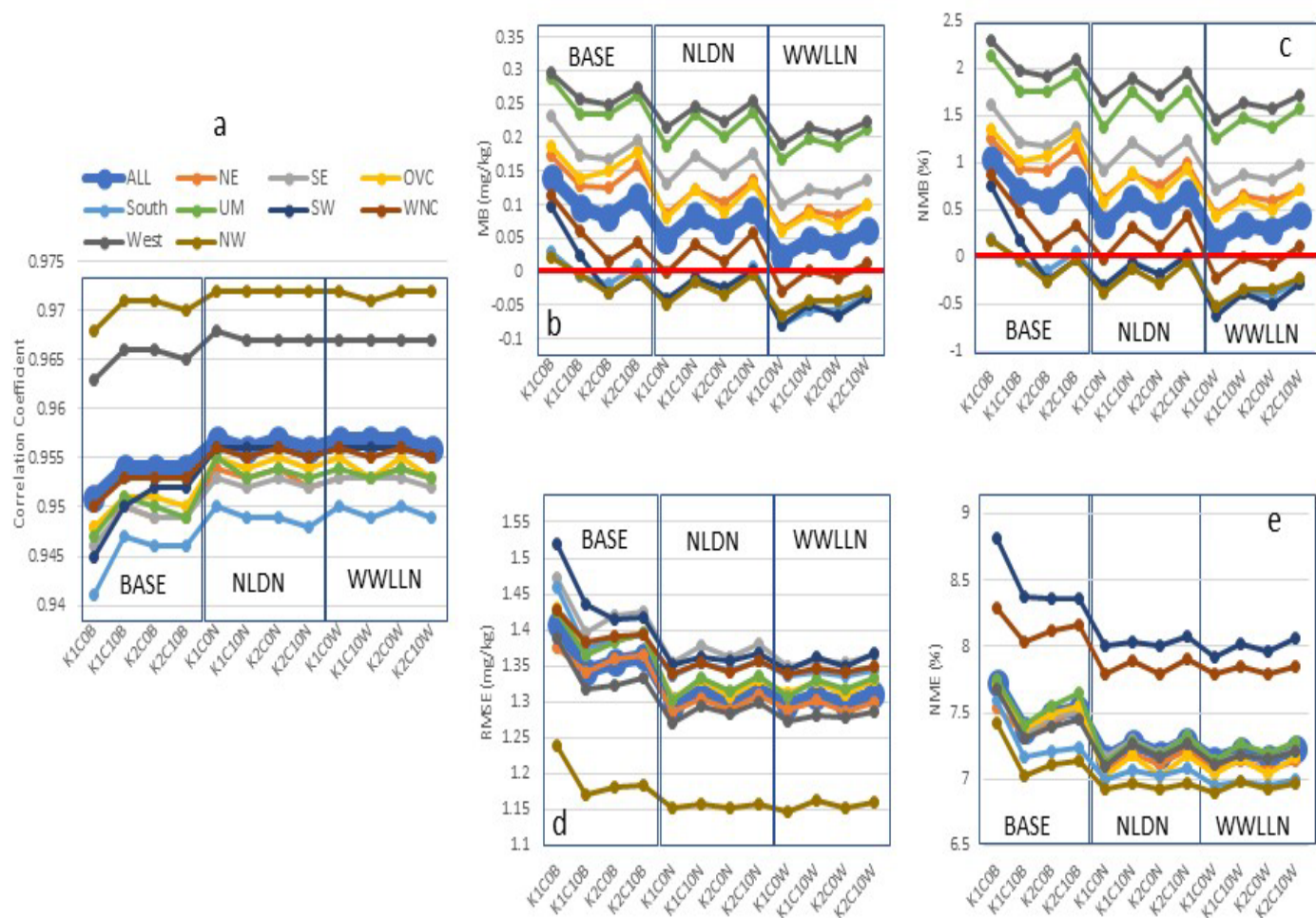
Figure 5. Same as Figure 4, but for 2-m water vapor mixing ratio.

839

840
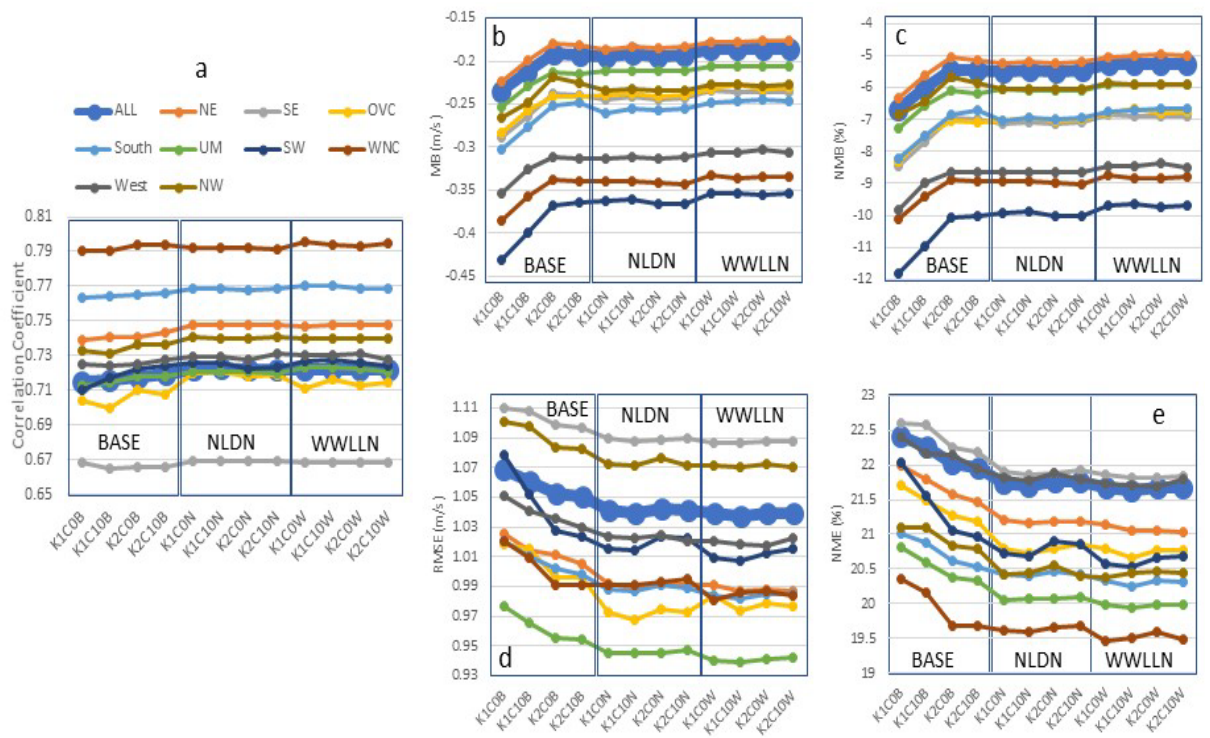
841

842 **Figure 6.** Same as Figure 4, but for 10-m wind speed.

843

844

845

846

847
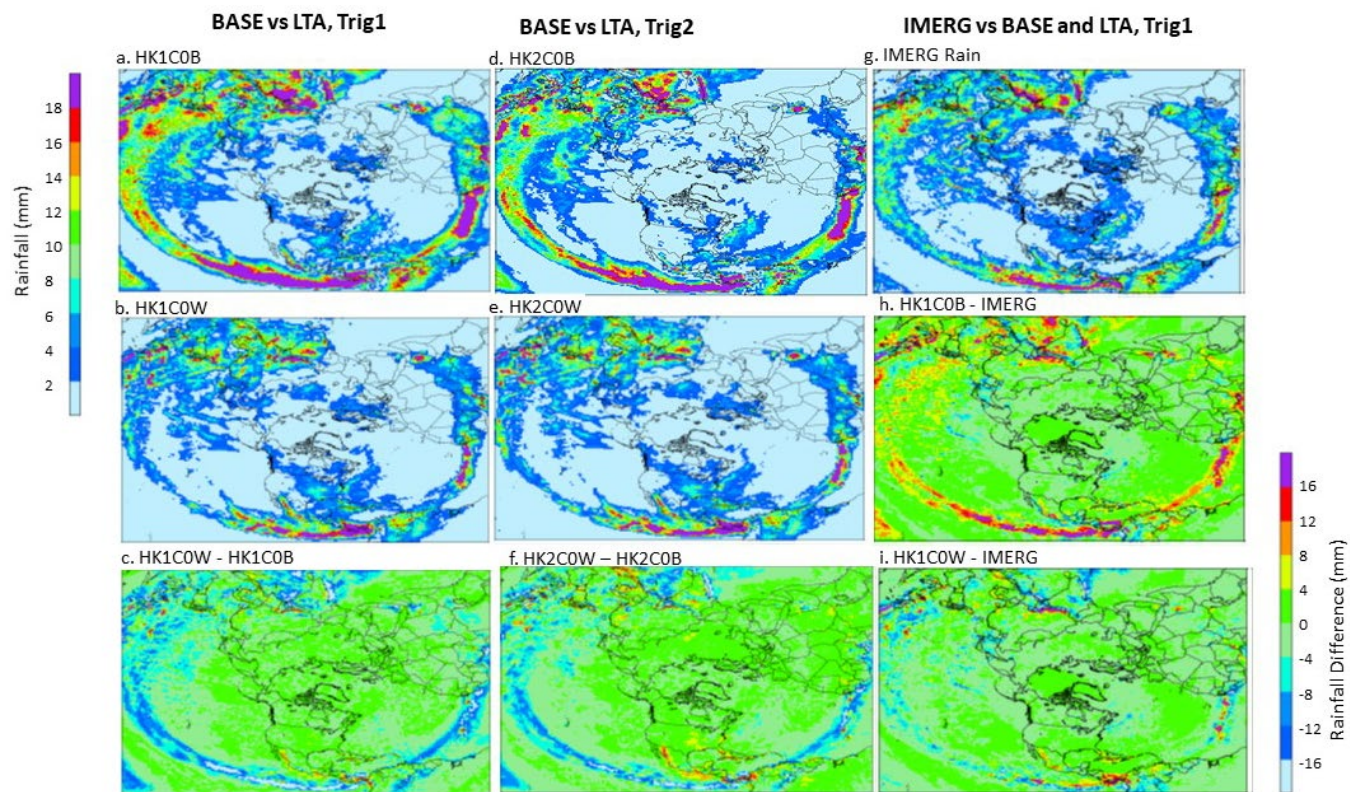
Figure 7. The mean daily rainfall during July 2016 simulated by base model cases (a. HK1C0B and d. HK2C0B), LTA cases (b. HK1C0W and e. HK2C0W), and the satellite GPM produced rainfall (g), and the differences between the LTA and BASE cases (c. HK1C0W – HK1C0B and f. HK2C0W – HK2C0B) and between the simulated cases and satellite IMERG products (h. HK1C0B – IMERG and i. HK1C0W – IMERG). Note that the left legend applies to the rain maps (a, b, d, e, and g), and the right legend applies to the difference plots (c, f, h, and i).

855
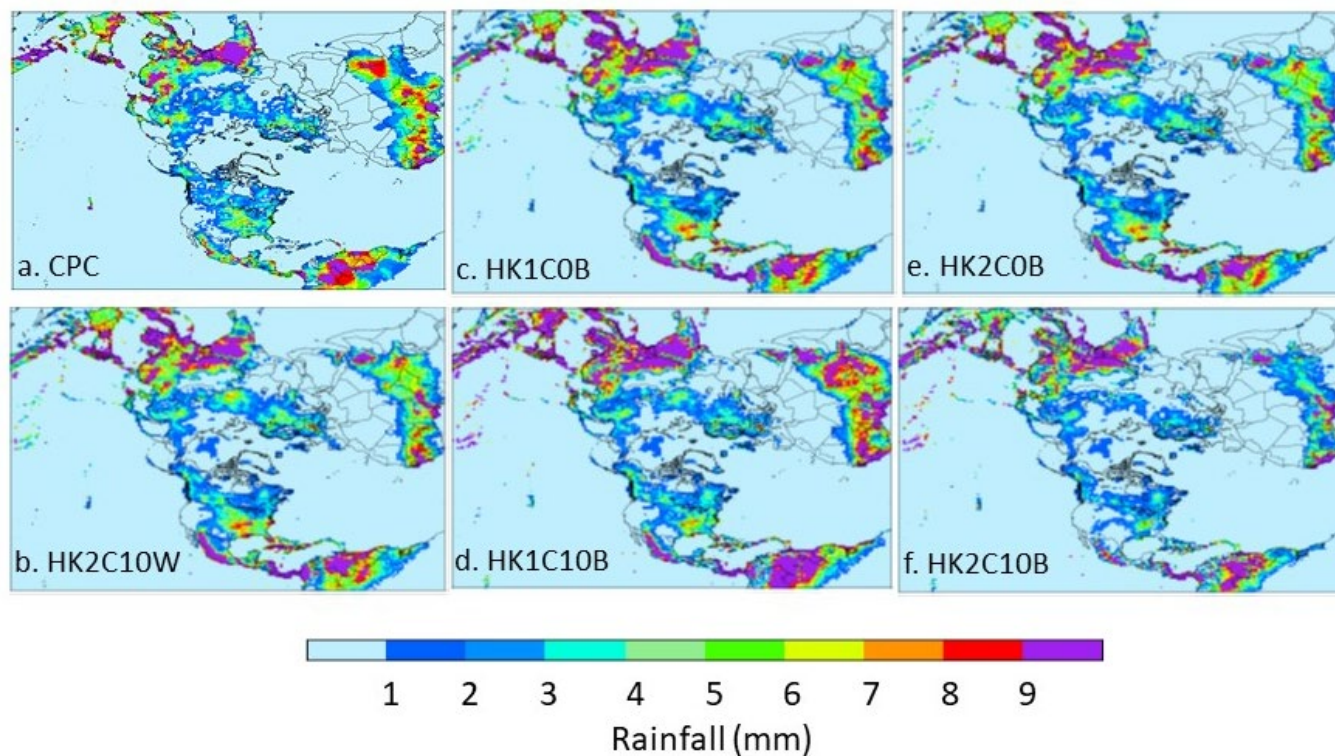
Figure 8. CPC rainfall (a) and simulated (b-f) mean daily precipitation during July 2016 over the hemispheric domain. The LTA configuration is represented by one case (b. HK2C10W) since all the LTA cases with different cumulus parameters produced similar results. All BASE cases are shown here (c-f) because the cumulus parameters do impact the simulated precipitation when not using LTA.

863

864
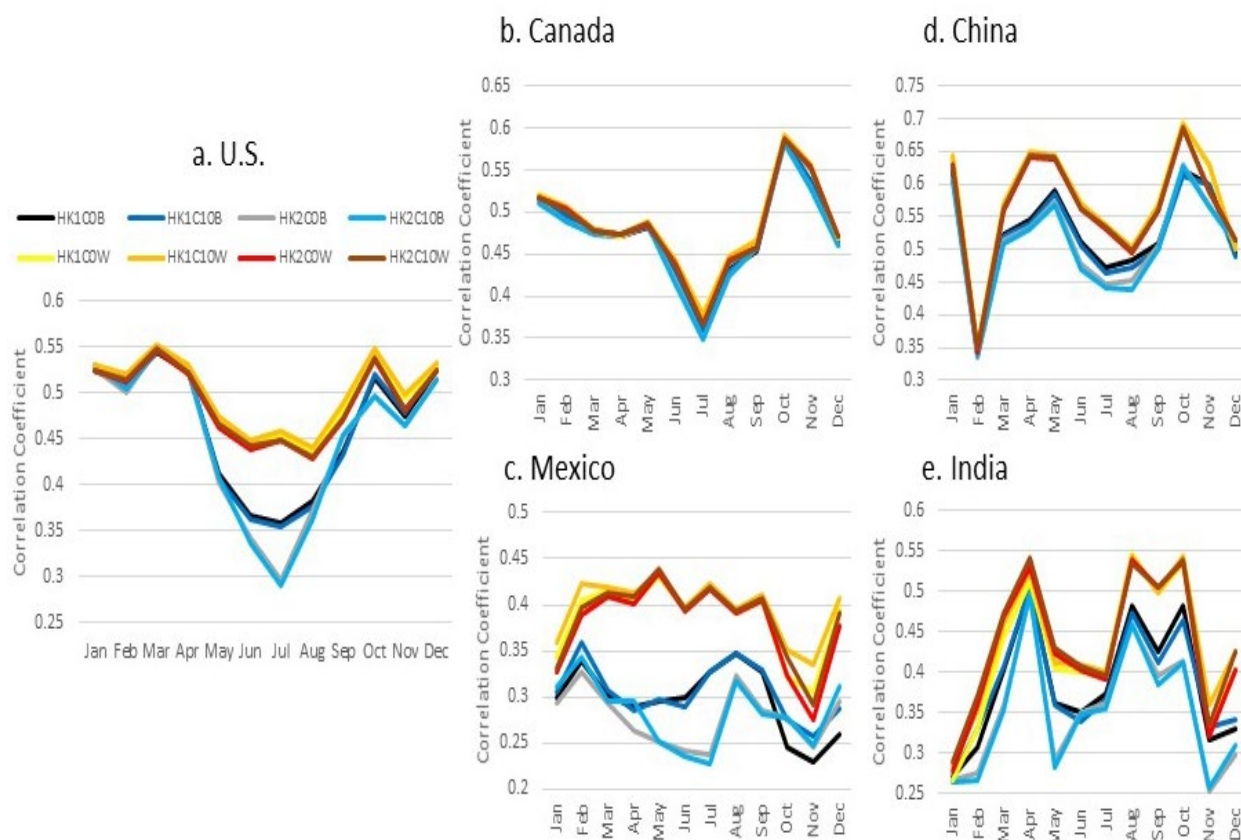
865

866 **Figure 9.** The monthly correlation coefficient between CPC and simulated precipitation in
867   selected countries: a. United States, b. Canada, c. Mexico, d, China, and e. India. Note
868   that all the BASE cases are plotted in cool colors and LTA cases in warm colors.
869

870

871
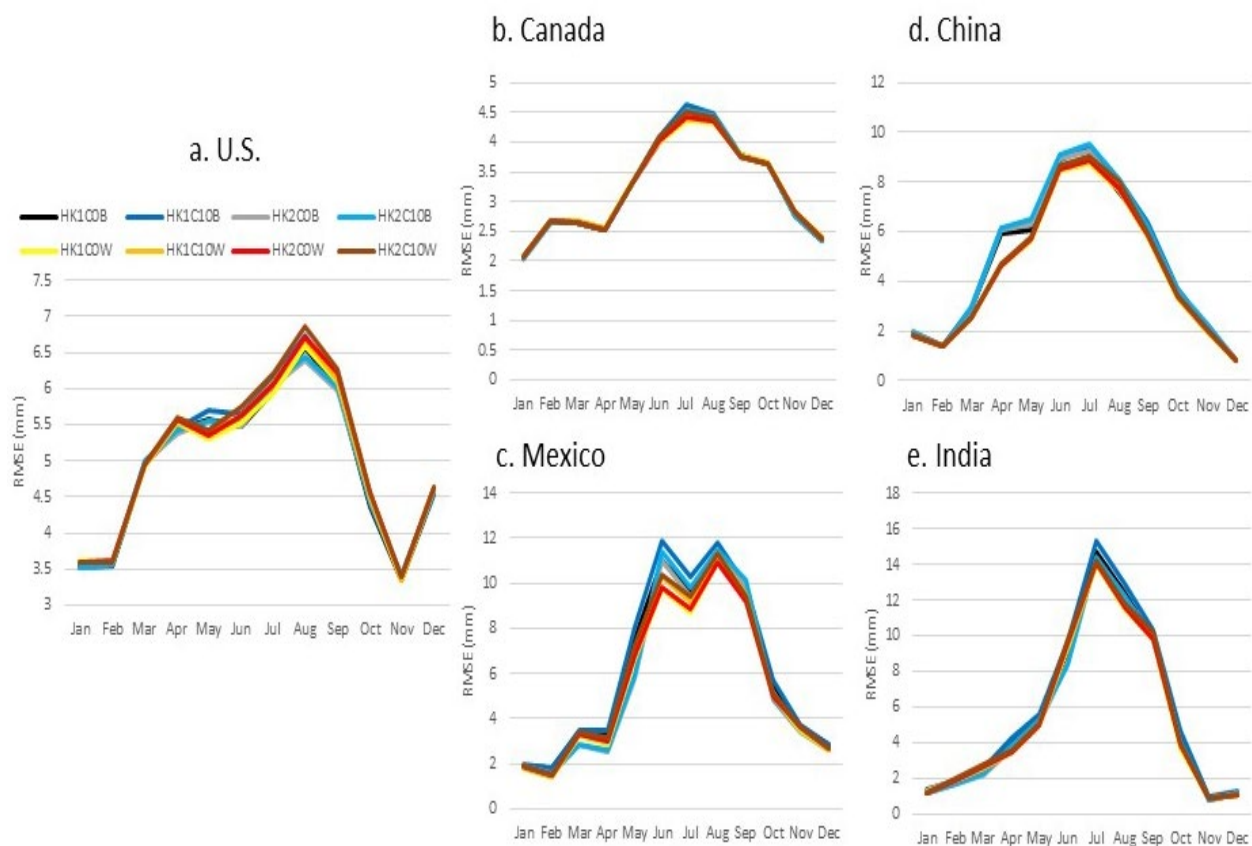
Figure 10. Same as Figure 9, but for RMSE.

873

874
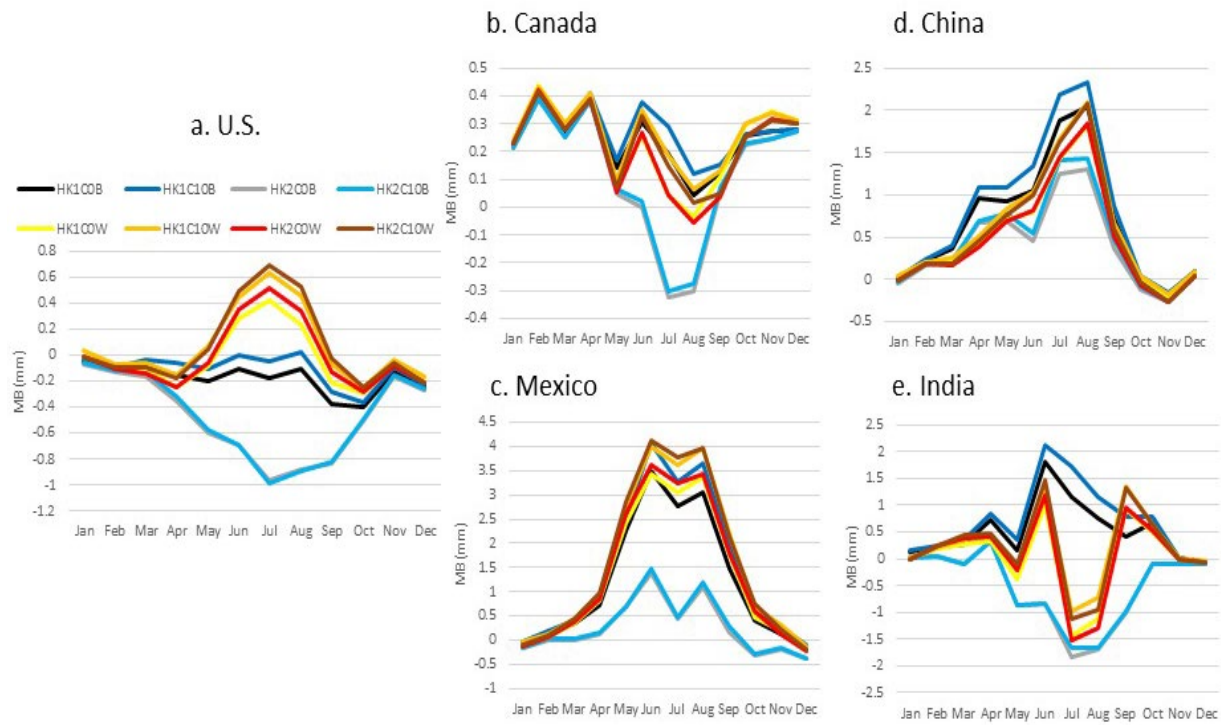
875

876 **Figure 11.** Same as Figure 9, but for MB.

877

878
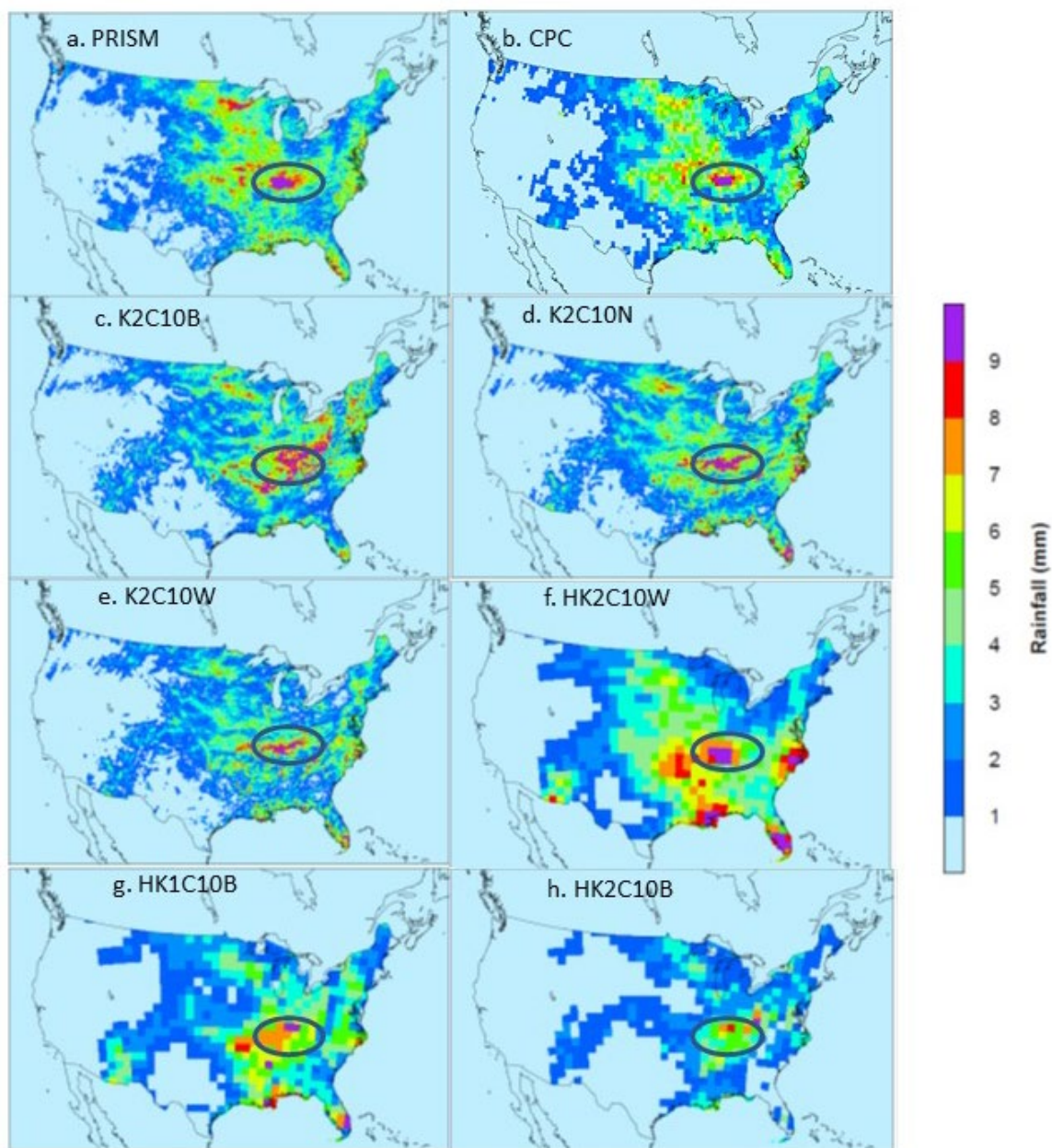
879

880   **Figure 12.** Mean daily precipitation over the CONUS during July 2016 from a) PRISM, b) CPC,
881   c) K2C10B, d) K2C10N, e) K2C10W, and f) HK2C10W, g) HK1C10B, and h)
882   HK2C10B. Note that all the observational based products and the 108 km hemispheric
883   simulations are regridded onto the 12 km CONUS domain.
884

885
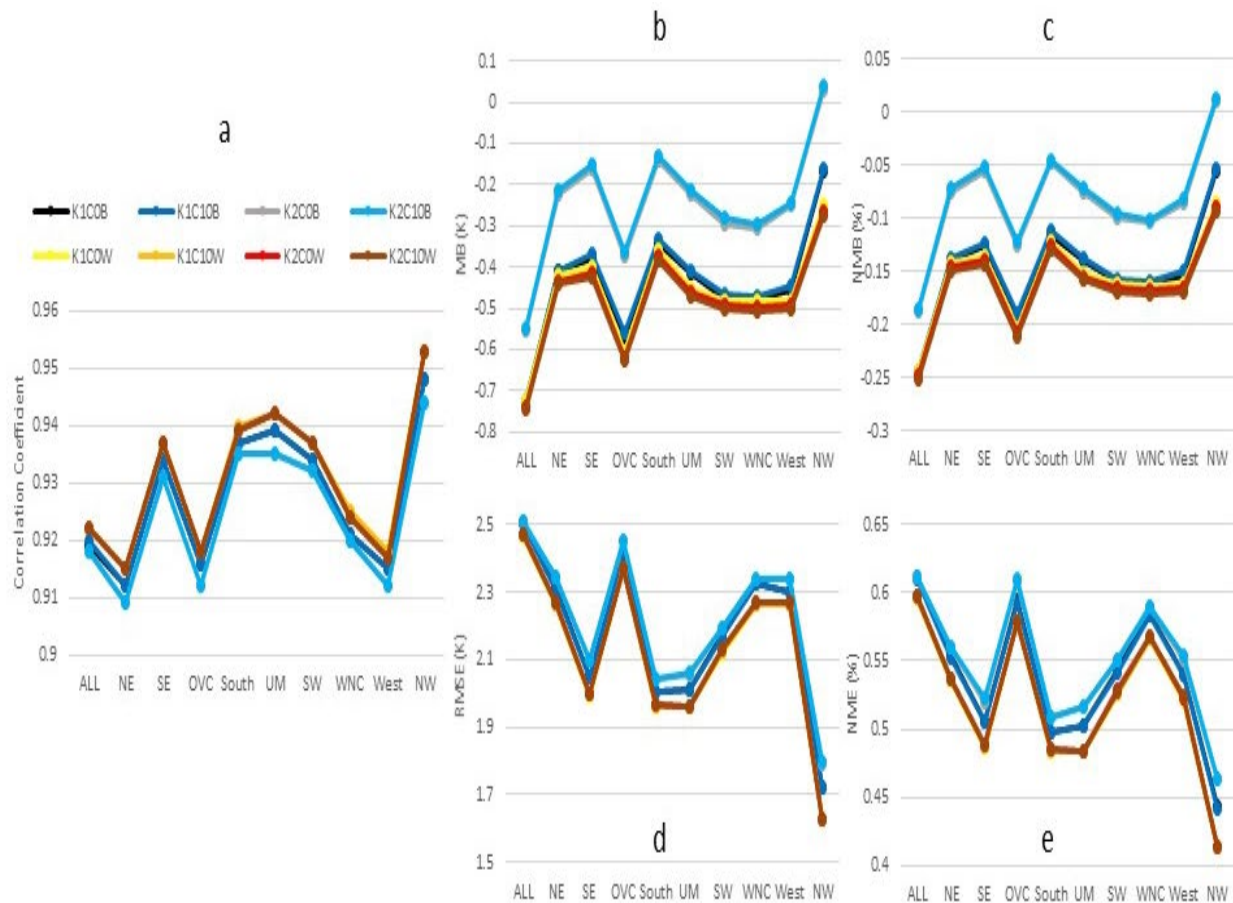
886

887 **Figure 13.** Monthly mean statistics for 2-m temperature from hemispheric BASE and LTA
888 simulations comparing to surface observations during July 2016: a) correlation coefficient, b)
889 MB, c) NMB, d) RMSE, and e) NME.
890
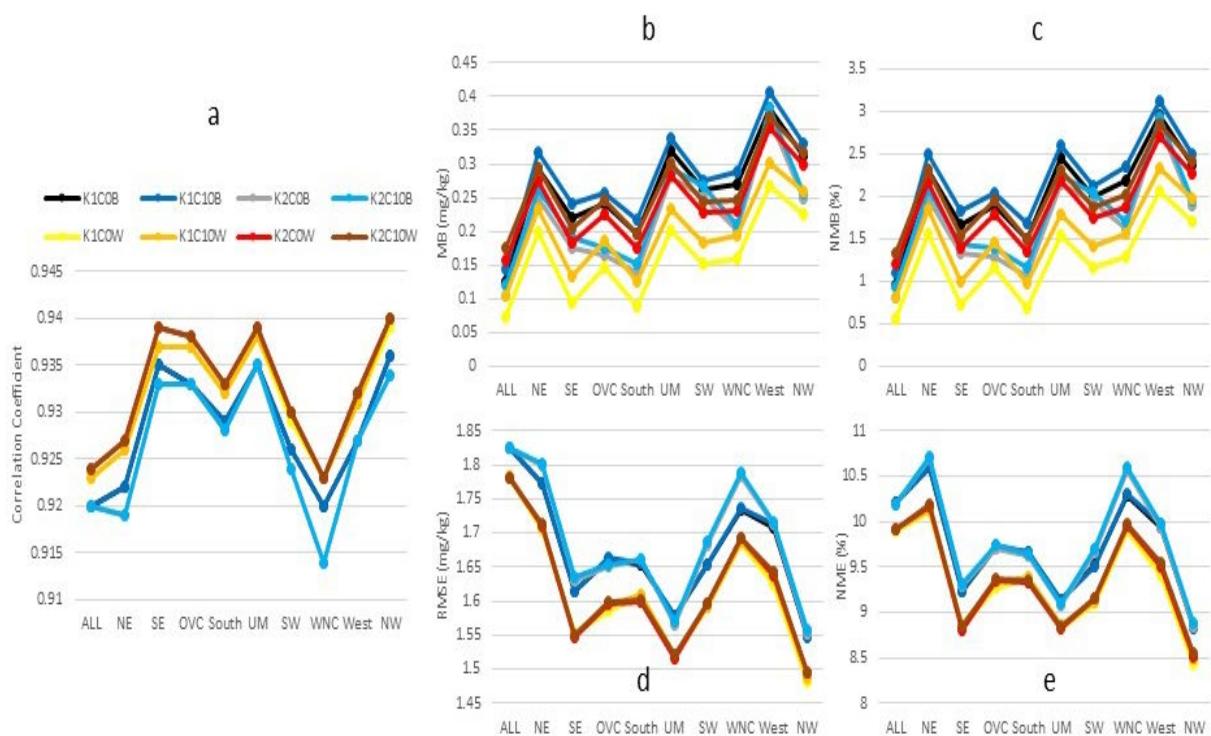
Figure 14. Same as Figure 12, but for 2-m water vapor mixing ratio.